A STEP TOWARDS CLOSED-LOOP CONTROL OF CHITOSAN DEGRADATION: CONJOINT THERMAL AND ENZYMATIC EFFECT, MODELING AND SENSING

A Thesis Submitted to the College of

Graduate Studies and Research

In Partial Fulfillment of the Requirements

For the Degree of Master of Science

In the Department of Biomedical Engineering

University of Saskatchewan

Saskatoon

By

Li Zhou

September 2011

Permission to Use

In presenting this thesis in partial fulfilment of the requirements for a Postgraduate degree from the University of Saskatchewan, I agree that the Libraries of this University may make it freely available for inspection. I further agree that permission for copying of this thesis in any manner, in whole or in part, for scholarly purposes may be granted by the professor or professors who supervised my thesis work or, in their absence, by the Head of the Department or the Dean of the College in which my thesis work was done. It is understood that any copying or publication or use of this thesis or parts thereof for financial gain shall not be allowed without my written permission. It is also understood that due recognition shall be given to me and to the University of Saskatchewan in any scholarly use which may be made of any material in my thesis.

Requests for permission to copy or to make other use of material in this thesis in whole or part should be addressed to:

Head of the Department of Biomedical Engineering

University of Saskatchewan

Saskatoon, Saskatchewan (S7N 5A9)

ABSTRACT

In scaffold-based tissue engineering, control of scaffold degradation turns out to be a critical issue for reliable clinical applications. Degradation in this thesis refers to mass loss. Most of the present control methods take the approach of scaffold material modification and/or scaffold work environment adjustment to address this issue. The latter can easily get to its limit, and the former is not promising in the *in-vivo* implementation. This thesis proposed a new approach to control of scaffold degradation, that is, closed-loop and real-time control. To realize this approach, this thesis has tackled three important problems, namely (1) effects on degradation, (2) modeling of degradation, and (3) real-time measurement of degradation. This thesis is grounded to a biomaterial called chitosan, as it is widely used for building scaffolds.

For the first problem, a statistical experiment was designed and a factorial analysis was conducted. For the second problem, a combined empirical-based and probabilistic-based approach was taken. For the third problem, a prototype of a sensor, which is based on the concept of carbon nanotube (CNT) conductive polymer, was built and tested. This thesis concludes (1) a joint thermal and enzymatic effect is significant on chitosan degradation, (2) the model for chitosan degradation is accurate, and (3) real-time measurement of mass loss of scaffold by means of carbon nanotube film is feasible.

The major contributions of this thesis are (i) the proposal of the concept of the closed-loop control of degradation, (ii) a finding that there is a significant conjoint thermal and enzymatic effect on chitosan degradation in terms of mass loss, and (iii) a prototype of the novel CNT

(carbon nanotube) chitosan film sensor for real-time measurement of mass loss of the scaffold. The significance of these contributions is that they give us confidence to a full development of the closed-loop and real-time degradation control approach. This approach appears promising to bring forth a transformative impact to clinic applications of scaffold-based tissue regeneration.

ACKNOWLEDGMENTS

I would like to express my heart-felt thanks to Professor W.J. (Chris) Zhang and Professor H. (Catherine) Niu for their esteemed guidance and endless support during this thesis work. I am also grateful to Professor W. J. (Chris) Zhang and Professor X.B. (Daniel) Chen for the financial support from NSERC (Natural Science and Research Council of Canada) and SHRF (Saskatchewan Health Research Foundation) and Professor H. (Catherine) Niu, and Professor L.Y. (Lily) Wu for the technique support during my study.

I would also like to express my gratitude to my committee members, Professor Assem Hedayat and Professor X.B. (Daniel) Chen for their valuable suggestion during my committee meeting.

I thank Mark Li, Ning Zhu, Paul Miao, Qian Huang, Hai-Dong Wang, Ki-Yong Song, Forrest Zhang, Shrey Modi, Kevin Yang, Sofia Shen and Mogen Thomas, for the various brainstorming sessions that helped me solve various issues relating to my thesis. I extend my thanks to all the members of Advance Engineering Design Laboratory group for their priceless suggestions during various seminars. I am also thankful to my roommates and very special friends, Shan Jin, Xin Yan, Mindan Wang, Zhubing Li, Nikki Janzen, Donica Janzen, Kara, Peter Shaw, Lucy Lu, Cam Janzen, Gerry, Shirley, Douglas and Sheila for their support and entertainment in my hectic academic work schedule.

Last but not the least; I am grateful to my dearest father and mother for their support and constant belief in me.

DEDICATED TO MY DEAREST MOTHER

AND MYSTIC SHANGRI-LA

TABLE OF CONTENTS

LIST OF FIGURES

LIST OF TABLES

CHAPTER 1

INTRODUCTION

1.1 Motivation

This research was motivated by the application of biomaterial scaffolds in tissue engineering. Research of scaffolds in tissue engineering has significantly advanced over the past decade (Langer & Vacanti, 1993). Ten years ago, the story that injured tissues can be "reconstructed" by applying engineering principles and non-living materials sounded fantastical to the average people (Thompson *et al*., 1995). Today, more and more patients survive thanks to various forms of artificial organ therapy, and 20% of the population older than 65 in developed nations are likely to benefit from organ replacement technology during the remainder of their lives (Langer, 2007). The needs for such transplantable tissues to replace, restore or enhance organ functions are urgent. As of late 2008, tissue engineered products generated annual sales of nearly $1.5 billion (Khademhosseini *et al*., 2009).

In parallel with the development of new implanted products, their mass degradation and degradation rate control, especially real-time on-line or semi-on-line, becomes an important issue. The on-line control may also be called closed-loop control (illustrated in Appendix A). There are two reasons to boost up the interest of on-line degradation control. First, products made of biomaterials are put in human body to play roles in

providing an environment for tissues to grow. The biodegradation of the biomaterials has direct effects on the growth of tissues. Second, it is both challenging and costly to develop a biomaterial whose degradation control is based on an open-loop control mechanism; adapted from comment in (Lee & Mooney, 2001; Ratner *et al*., 2003; Khademhosseini *et al*., 2009; Langer, 2007). Here, the phrase 'closed-loop control' of biomaterial degradation is called 'control' for simplicity.

In order to effectively control the degradation of biomaterials, understanding of their degradation mechanisms under a certain environment and development of sensors that can measure degradation rate are two primary tasks (Hu *et al*., 2010). The thermal effect is potentially a viable approach to degradation control, so understanding of the thermal effect on degradation of biomaterials was one of the issues for this thesis. Another issue concerned in this thesis was to measure degradation rate in real-time, for which carbon nanotube may have a high potential, owing to its general promise to be a biosensor. The biomaterial concerned in this thesis is chitosan which is a natural biomaterial and has promise in tissue regenerative medicine.

1.2 Objectives

This research aimed to address the aforementioned issues and in particular to underatand thermal effect with enzymatic treatment in degradation, degradation

predication, and degradation measurement. Three specific research objectives were then proposed for the thesis, and they are described below:

Objective 1*: Study the thermal and thermal-enzymatic degradation behaviors of chitosan films in a proper temperature range*. The specific enzyme used is lysozyme, which has a significant effect on chitosan degradation according to the current literature (Hirano & Mooney, 2004). Note that the temperature ranges from 37°C to 50°C, which is considered as a "safe" range for human body. The particular goal of this thesis study was to examine whether thermal effect and thermal-enzymatic effect are significant. The study on this objective is crucial, as only when these effects are significant, can they be employed to control degradation. It is noted that, however, a preliminary investigation did provide some confidence on these effects, which led us to propose the second objective for this thesis research in the following.

Objective 2*: Develop a degradation model with consideration of a conjoint thermal and enzymatic effect*. As implied in the above discussion, research on this objective depends on the outcome of the first objective. It is likely that the model contains the temperature, enzyme, time as independent variables and a particular measure for degradation is molecular mass loss and it serves as a dependable variable. It is noted that the properties of chitosan including its molecular mass will be discussed in Chapter 2 of the thesis. The usefulness of such a model is two-fold: (1) helpful to closed-loop control in future, because the model can serve as a plant dynamic model

which is important to control, and (2) helpful to new biomaterial development or existing biomaterial modification.

Objective 3*: Explore real-time measurement of degradation of chitosan films or scaffolds*. During the degradation control process, real-time measurement of degradation is a crucial part. The quantity to be measured is mass loss, and the reason to choose this property will be discussed in Chapter 2. It is noted that though the ultimate goal is to measure mass loss *in-vivo*, the current study is restricted to *in-vitro* measurement.

It is worth to point out that this research, as described with the three objectives above, was intended to provide a part of the entire closed-loop and real-time control system for degradation. The issues such as degradation information or signal processing, thermal and enzymatic delivery to human body, and so on were out of the scope of this research.

The outcomes of this research are (1) a better understanding of the thermal effect on the degradation of chitosan, (2) a model that can predict the degradation of chitosan based on the thermal effect treated with enzyme, and (3) a feasibility of a sensor for measuring degradation of chitosan in real-time.

1.3 Research Method

With respect to Objective 1, an experimental approach was taken. In particular, the statistical design of experiments (DOE) was conducted in order to cope with inherent uncertainties existing in biological systems. With respect to Objective 2, a regression method was employed. As well, a Monte Carlo technique was used for simulating the degradation process, owing to the randomized nature of tissue growth in the context of scaffold. Finally, with respect to Objective 3, multi-wall carbon nanotube (MCNT) was employed to follow a spin coating process to fabricate CNT film (Jo *et al*., 2010), mixed up with chitosan. The film is conductive, and it is thus called CNT-Chi film hereafter. It is noted that the statistical knowledge uesd in this thesis, Monte Carlo simulation technique, and a brief introduction of CNT, are presented in Appendix B, Appendix C and Appdendix D, respectively, for the convenience of readers.

1.4 Thesis Organization

The remainder of this thesis is laid out to six more chapters as follows:

Chapter 2: This chapter will introduce basic knowledge of tissue engineering, scaffold, biomaterial, degradation, and degradation control in literature. Upon the basic knowledge, this chapter will also describe the state of knowledge of biomaterial

degradation control so that the proposed research can be more justified for its need and novelty.

Chapter 3: This chapter studies the thermal effect and conjoint thermal and enzymatic-thermal effect on chitosan degradation. This chapter presents the work towards Objective 1. In particular, this chapter includes the design of experiment, results, discussion, and conclusion.

Chapter 4: This chapter will develop a model for degradation estimation and predication. This chapter presents the work towards Objective 2. In particular, this chapter includes a detailed methodology to develop the model and the model validation.

Chapter 5: This chapter will present a preliminary study for the CNT-based sensor development to measure mass loss of chitosan scaffold. This chapter presents the work towards Objective 3. This includes the requirement analysis for such a film-sensor, design and fabrication of the film-sensor, and validation of the sensor.

Chapter 6: The final chapter discusses the contributions, limitations and future work.

CHAPTER 2

BACKGROUND AND LITERATURE REVIEW

2.1 Introduction

In this chapter, some important background and state of knowledge of biomaterial degradation will be discussed. The goal of the discussion is to further justify the need and novelty of the proposed research as well as to provide some context for subsequent discussions. Section 2.2 presents the basic concept of tissue engineering and scaffold. Section 2.3 discusses biomaterials for scaffold. Section 2.4 discusses chitosan which is focused by this thesis. Section 2.5 discusses degradation control including CNT and CNT-based sensors. Finally, Section 2.6 gives a conclusion on the proposed research defined in Chapter 1.

2.2 Tissue Engineering and Scaffold

Tissue engineering (TE) is a discipline to create or modify tissues to restore, maintain, or improve various functions of the tissues (Langer & Vacanti, 1993). Creating new tissues is important because organ transplants are severely hampered by shortage of donors. For instance, approximately 30,000 patients in the United States die annually of liver failure, with less than 3000 transplants available (Langer, 2000).

Regeneration of tissues needs a physical container called scaffold which is made of biocompatible materials e.g., chitosan. The scaffold provides a support to cells so that the cells can be placed at the site of concern in human body and then grow (Stock & Vacanti, 2001). Examples of the site are skin, cartilage, tendon, liver, oesophagus, cardiovascular structures, intestine and bone, and artificial tissues such as bladder, cornea, bronchial tubes, blood vessels (Bianco & Robey, 2001). Two examples in skin and bone regeneration are shown in Fig. 2.1.

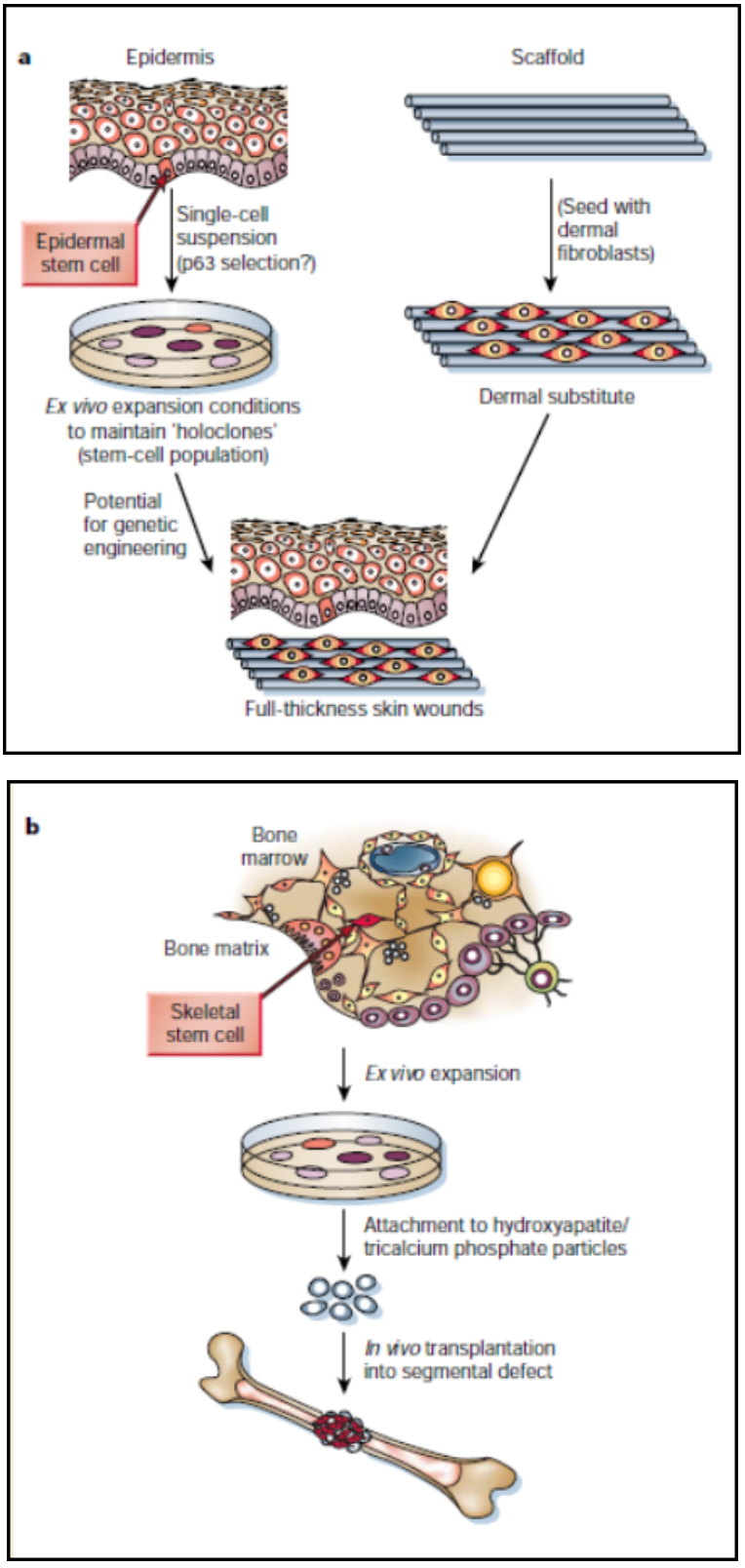

Figure 2.1. Regeneration of (a) two-dimensional (skin) and (b) three-dimensional (bone) tissues using stem cells (Bianco & Robey, 2001).

Although significant advances over the past decade have come from new insights into the way the body naturally builds tissues, obstacles remain (Lee & Mooney, 2001). First, scaffolds built with the existing materials are difficult to control regarding their property change, e.g., degradation (Rivest *et al*., 2007). Second, both research into new materials and investment of the new materials seem to be costly and time consuming. This situation has boosted up research on control of degradation of biomaterials in many ways, among which modeling and prediction approaches are widely studied (Siepmann & Göpferich, 2001). However, these approaches are at most open-loop control and thus highly limited in biological systems. To the best of author's knowledge, nobody seems to embark on any research on the idea of the closed-loop control of degradation especially with thermal effect.

2.3 Biomaterials for Scaffold

A widely agreed definition of biomaterial is that a biomaterial is a material that can interact with biological environments and can be used in medical fields (Lendlein & Langer, 2002). Biomaterials can be divided into four major classes of materials: polymers, metals, ceramics (including carbons, glass-ceramics, and glasses), and composite material (gained by combining two different classes of materials together) (Ratner *et al*., 2003).

Particularly, biopolymers have two categories: natural and synthetic. Natural polymers are derived from renewable resources, namely from plants, animals and microorganisms, and are, therefore, widely distributed in nature, e.g. chitosan and chitin. Synthetic biomaterial is synthesized from polymers, e.g. poly(lactic acid) (PLA).

The advantage of biomaterial is its biodegradability, biocompatibility, and proper physical attributes to be made into whatever form desired (Vacanti *et al*., 2006). Applications of biomaterial include tissue scaffold fabrication (Langer, 2000). One example of such applications is cartilage, where a small sample of cartilage was extracted into cartilage cells from an animal and the cartilage cells were then multiplied on a human ear shape PLA scaffold in a bioreactor (Avraham *et al*., 1994). The PLA-based cell scaffold was grafted onto mice in that specific anatomic shape (Carrier *et al*., 1999). In another example, skin with burns or skin ulcers were repaired by placing dermal fibroblasts on poly(lactic-co-glycolic acid) (PLGA) scaffolds and the injured skin was then grown into sheets (Hauft *et al*., 1992).

Several requirements have been identified as crucial for the tissue scaffolds (Hutmacher, 2001): (1) to possess interconnecting pores with appropriate scales to favor tissue integration and vascularization, (2) to be made from materials with controlled biodegradability so that tissue can eventually replace the scaffold, (3) to have appropriate surface chemistry to favor cellular attachment, differentiation and

proliferation, (4) to possess adequate mechanical properties to match the intended site of implantation and handling, and (5) not to induce any adverse response.

The aforementioned physical and chemical properties are subject to change in the course of cell culture and tissue growth. This means that at one time, a scaffold may satisfy the requirements but as time goes on, it may deviate to dissatisfy the requirements. The most basic change is naturally its structural change, such as weight (mass) or architecture. This thesis focused on changes in mass and calls it degradation. Indeed, in literature, degradation seems to imply mass loss. This thesis was based on the author's observation that the degradation behavior of the biomaterial-based scaffold is not controllable in a closed-loop fashion nor monitored by any real-time approach in the contemporary literature.

2.4 Chitosan as Biomaterial in Tissue Engineering

2.4.1 Structure

Chitosan is a structural polysaccharide, which is derived by deacetylation of the N-acetyl-D-glucosamine unit from chitin (Fig. 2.2). In particular, when chitin is deacetylated to about 50% of the free amine units, it is referred to as chitosan (Vårum *et al*., 1997). In nature, chitosan is found in dimorphic fungi such as *Mucor rouxii* wherein it is formed by deacetylation action of a deacetylase enzyme on chitin. In

industry, chitosan is formed from a deacetylation process of chitin after obtaining chitin from shrimp and crab shells.

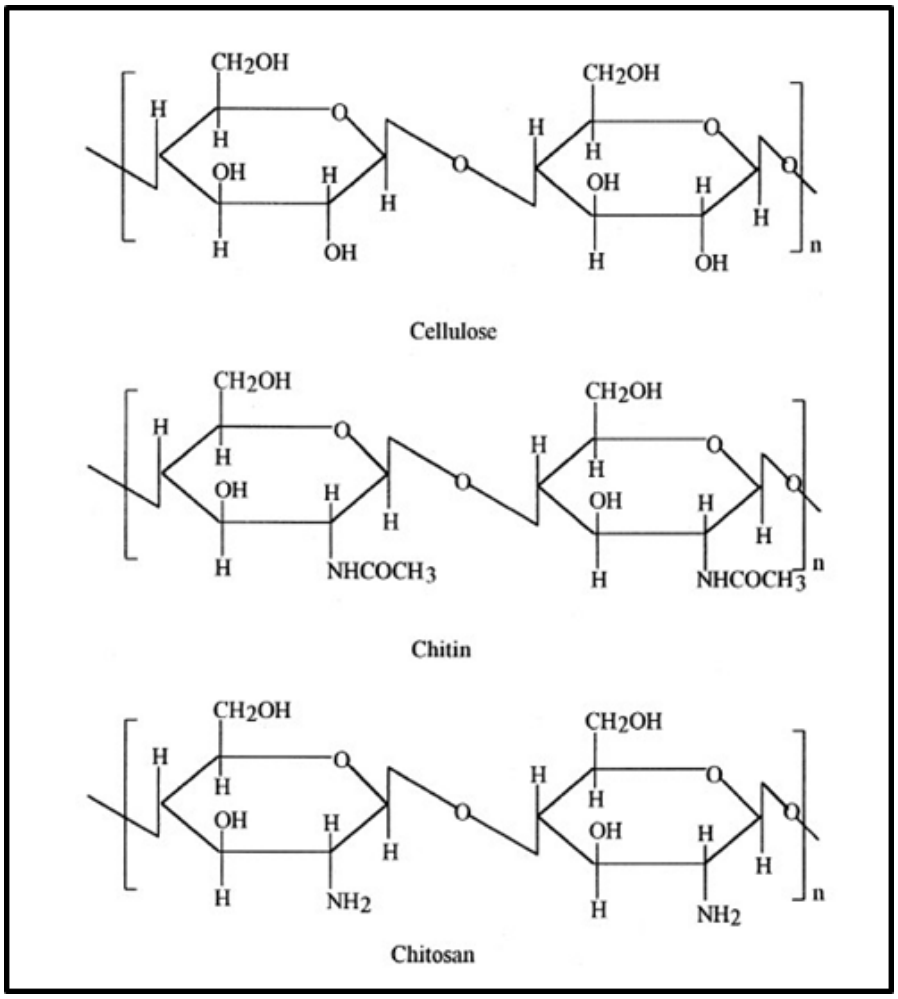

Figure 2.2. Chemical structures of cellulose, chitin and chitosan (Kumar *et al.*, 2004).

As a natural polymer, chitosan shows a high quality of biocompatibility, non-toxicity, bio-adhesive property, and biodegradability (Kumar *et al.*, 2004). As a structural polysaccharide, chitosan has a relatively higher mechanical strength than other natural biomaterials. Therefore, pure chitosans or chitosan-based composite polymers are materials which are widely used for making scaffolds.

2.4.2 Properties

Molecular weight (MW). The molecular weight, also called the relative molecular mass of chitosan, represents the ratio of the mass of that molecule of chitosan to 1/12th of the mass of carbon-12 molecule and is a dimensionless number. The molecular weight affects the chemical and physical properties of chitosan. Molecular weight of chitosan ranges from 50 to 1000 kDa (Francis & Matthew., 2000). Chitosan molecular weight distributions can be obtained using HPLC. The weight average molecular weight (M_W) of chitin and chitosan can be determined by light scattering. A simple and rapid method for the determination of molecular weight is using viscometer. The molecular weight is calculated by the Mark-Houwink equation (Kumar *et al*., 2004):

$$[\eta] = KM^{\alpha} = 1.81\times10^{-3}M^{0.93} \quad (2\text{-}1)$$

where α and K are constants and are determined in 0.1 M acetic acid and 0.2 M sodium chloride solution, respectively.

Degree of deacetylation (DD). The degree of deacetylation represents the proportion of N-deacetyl-D-glucosamine units in the total number of units, and it ranges from 50% to 100%; see Fig. 2.3. The degree of deacetylation (DD) can influence both the chemical and physical properties of chitosan. For instance, the DD is related to the

crystalinity of chitosan, which would affect the biodegradation rate of chitosan (Vårum *et al*., 1997). Fourier Transform Infrared (FT-IR) spectrometry is usually used to determine the DD of the chitosan. It is noted that chitosan has nitrogen content higher than 7% and degree of acetylation lower than 0.40. Removal of the acetyl group is a harsh treatment usually performed with a concentrated NaOH solution (either aqueous or alcoholic).

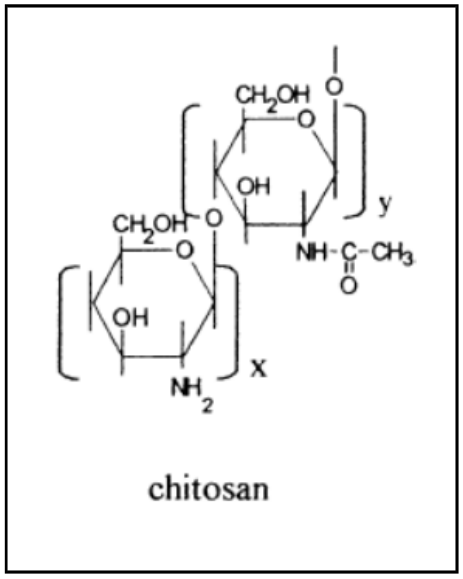

Figure 2.3. Chitosan chemical structure (Vårum *et al*., 1997).

Solubility. Chitosan is a primary aliphatic amine that can be protonated by selected acids, and the pKa of the chitosan amine is 6.3. The following salts, acetate, lactate, malate, citrate, glyoxylate, pyruvate, glycolate, and ascorbate, are water soluble.

2.4.3 Applications

Scaffold. One of the chitosan's most promising features is its excellent ability to be produced into porous structures for use in cell transplantation and tissue regeneration (Ratner *et al.,* 2004). Chitosan scaffolds have promising mechanical stiffness and have good mechanical properties (Kumar *et al.*, 2004). Porous chitosan structures can be formed by freezing and lyophilizing chitosan salt solutions in suitable molds (Illum, 1998). Francis and Matthew (2000), recently, reviewed the application of chitosan-based polysaccharide biomaterials in cartilage tissue engineering. Chitosan biocompatibility was investigated in the mice model by implantation of porous chitosan scaffolds and their evaluation. Madihally and Matthew (1999) studied bulk scaffolds and also performed systematic studies demonstrating the effects of freezing temperature and chitosan concentration on the mean pore diameter of cylindrical chitosan scaffolds. Bulk scaffolds were also prepared in a planar geometry by freezing chitosan solutions in shallow dishes, resulting in a planer scaffold which is 5 mm thick with perpendicularly oriented, thin walled pores. The mean pore diameter can be controlled within the range of 40-250 μm by varying the freezing temperature and hence the ice crystal size. Chitosan scaffolds support the attachment, morphology, and proliferation of various kinds of cells, including chondrocytes and dermal fibroblasts.

Film. Chitosan possesses good film-forming properties, and an update on chitosan films for pharmaceutical applications is presented here. The choice of biomaterials

suitable for forming the carrier film matrix and the barrier film are dictated by various factors: (a) compatibility with the gastric environment, (b) stability during the time of drug delivery, (c) adequate mechanical properties, (d) ease of fabrication and cost, and (e) no appreciable swelling in water and softening point above 37°C.

Tomihata and Ikada (2000) reported *in-vitro* and *in-vivo* degradation profiles of chitin and chitosan films by the solution casting method using specimens of varied deacetylation degree; the thickness of the films was 150 μm. The equilibrated water content of the films decreased with increase in deacetylation, while the tensile strength of the water-swollen films increased with increase in deacetylation. The maximum water content and minimum tensile strength observed for a specimen deacetylated between 0 and 68.8 mol% may be ascribed to the lowered crystallinity by deacetylation of chitin, since both chitin and chitosan are crystalline polymers.

2.5 Degradation Control for Biomaterials

2.5.1 General concept of degradation control

An important behavior of biomaterial scaffold is that it degrades and resorbs at a rate that matches the formation of new tissue (Lyu *et al.*, 2007). The degradation and re-sorption kinetics of the scaffold follows the relationships of mechanical properties, mass loss and tissue development (Burkersroda *et al.*, 2002). Fig. 2.4 shows three

situations, i.e., too slow degradation (Fig. 2.4-A), balanced degradation and re-sorption (Fig. 2.4-B), and too fast degradation (Fig. 2.4-C).

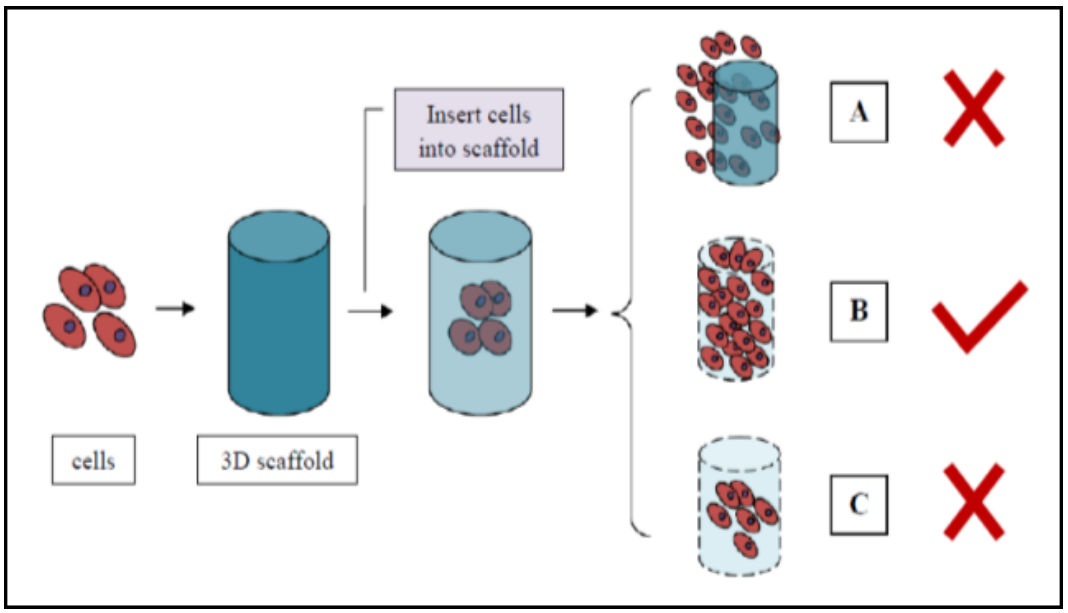

Figure 2.4. Scaffold degradation rate versus tissue regeneration rate. A: scaffold degradation rate is slower than tissue regeneration; B: scaffold degradation rate matches tissue regeneration rate; C: scaffold degradation rate is faster than tissue regeneration rate.

Degradation control is meant to regulate the degradation rate or process (Langer, 2007; Freier, 2005). By making an analogy to general dynamic system control, degradation control has open-loop or feed-forward and closed-loop or feedback control strategies (see Appendix A for general knowledge of dynamic system control). Open-loop controls rely on the effect and material dynamics, while closed-loop controls change the effect to lead to the change of material dynamics. Both control strategies share (1) effect, (2) model, and (3) measurement. It is noted that the current literature has no

work on the closed-loop strategy for degradation control, so in the following, the literature on the open-loop control strategy is reviewed only.

2.5.2 Degradation mechanisms and factors

The process of degradation is a chain scission process, during which polymer chains are cleaved to form oligomers and monomers. Since scaffolds are essentially in a wet environment, water plays an important role in this chain scission process; in particular water enters the polymer bulk, accompanied by swelling which then triggers the chemical polymer degradation (i.e., creation of oligomers and monomers). This water-induced process may also be called **hydrolysis**. When in a scaffold, oligomers and monomers form, they basically leave the body of the scaffold; the weight of the scaffold will then lose.

In addition to the hydrolysis processes, enzymes can also be a factor for biomaterial degradation, which is called **enzymatic hydrolysis** (Langer & Vacanti, 1993). The mechanism behind enzymatic hydrolysis is such that an enzyme plays a catalytic role during a water-induced hydrolysis process (Kumar *et al*., 2004). Take lysozyme for example. Lysozyme attacks peptidoglycans and hydrolyzes the glycosidic bond that connects N-acetylmuramic acid with the fourth carbon atom of N-acetylglucosamine (Yoshimura *et al.*, 1988). This process occurs by binding lysozyme to the peptidoglycan molecule in binding sites within the prominent cleft between its two

domains. This can further cause the substrate molecule to form a strained conformation. The lysozyme then distorts the fourth sugar in hexasaccharide (the D ring) into a half-chain conformation. In this strained and stressed state, the glysosidic bond is broken (Vocadio *et al.*, 2001). However, the enzymatic degradation can only happen with natural polymers such as polysaccharides and proteins (Langer, 2000).

There are several factors that influence degradation rate of polymers: type of chemical bond (liable bond) (Fig. 2.5), pH, and copolymer composition and water uptake. It is noted that chemical and physical changes go along with the degradation of biodegradable polymers, such as crystallization of oligomers and monomers and pH values, and so on; some of these factors can have a substantial backward effect on the degradation rate, e.g. water uptake (Suárez *et al.*, 1998).

.

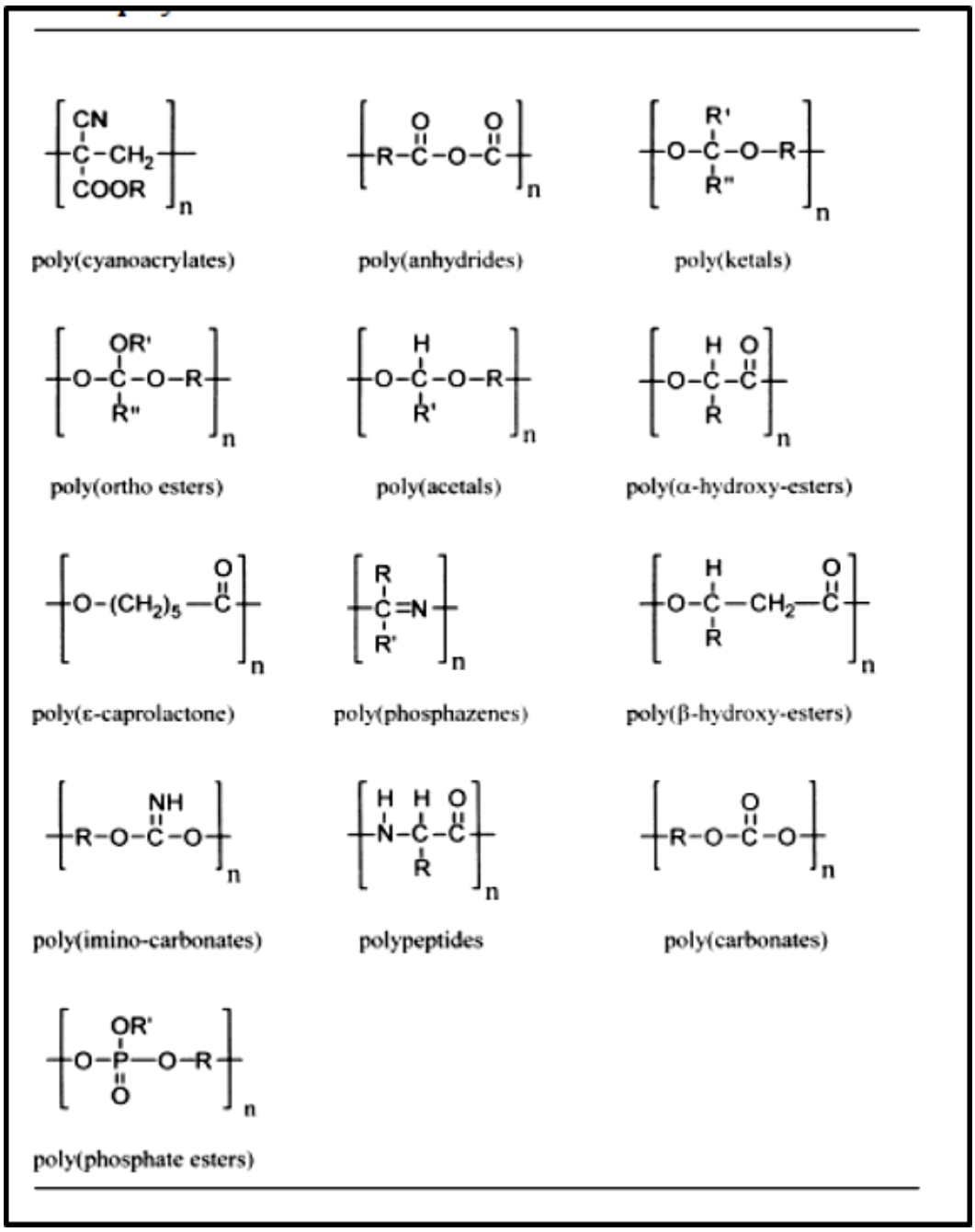

Figure 2.5. Liable bond (Siepmann & Göpferich, 2001).

An important parameter for monitoring degradation is molecular weight (Thompson *et al*., 2010). Besides loss of molecular weight, other parameters have been proposed as a measure for degradation as well, such as loss of bulk weight, loss of mechanical strength, complete degradation into monomers or monomer release, etc. Among these

parameters, mass loss is considered as the simplest and essential one (Soares & Zunino, 2010).

Degradation can be further classified into two kinds: surface degradation and bulk degradation (Langer & Peppas, 1983). Surface degradation is such that degradation mainly occurs in the outermost polymer layer, while bulk degradation is such that degradation occurs in the whole polymer volume in a simultaneous manner (Siepmann & Göpferich, 2001). Fig. 2.6 gives the schematic explanation of them. Further, surface degradation is much faster than water intrusion, while bulk degradation is much slower than water intrusion (Burkersroda & Göpferich, 1999). Generally speaking, surface degradation dominates among the polymer (which is built from very reactive functional groups); while bulk degradation dominates the less reactive functional groups. For instance, polyanhydrides is predominantly surface degradable, while poly(lactide) (PLA) and poly (lactide-co-glycolede) (PLGA) are bulk degradable. However, in reality, both of the degradations usually occur simultaneously but not at the same rate.

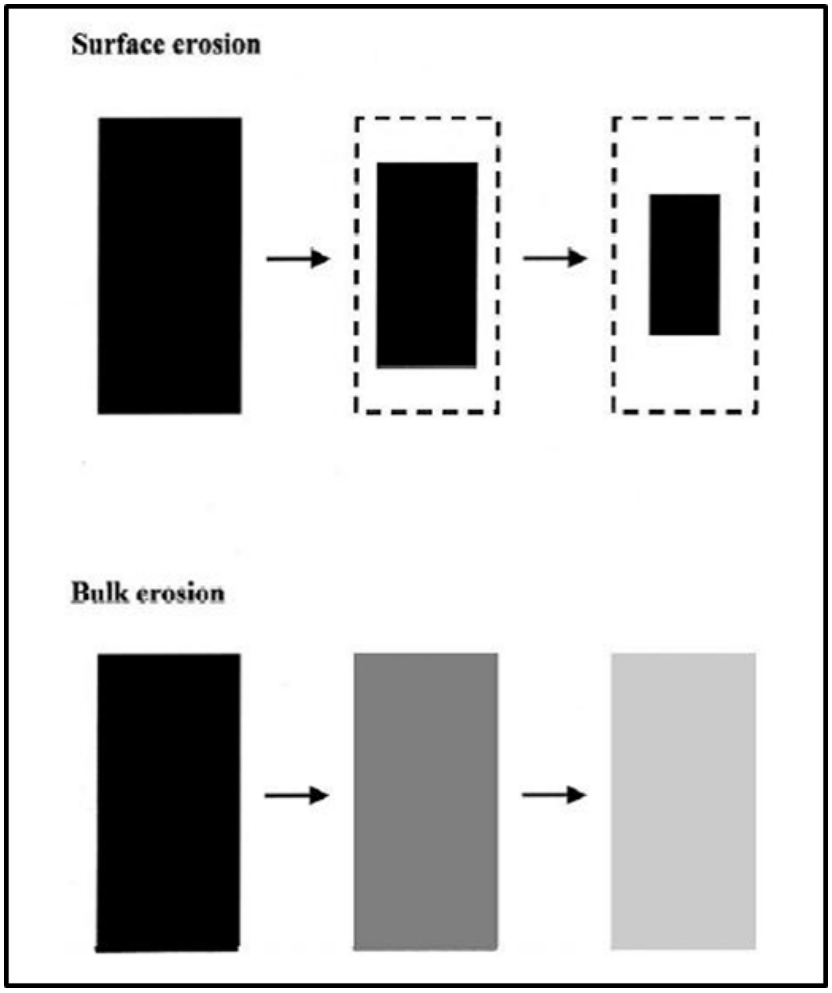

Figure 2.6. Schematic illustration of the principles of surface and bulk degradation (Siepmann & Göpferich, 2001).

In the current literature, degradation control is mainly on modification of the scaffold material and its work environment (Cunha-Reis *et al*., 2006). One of the important concepts as well as techniques is the so-called grafting critical chemical chain sequences on synthetic polymers. It is observed that the anhydrides accelerate hydrolysis through acid catalysis (Langer, 2000). Some other techniques are such as changing pH of degradation environments (Göpferich, 1997), adding growth factors into scaffold material (Huebsch & Mooney, 2001), and changing the polymer matrix

structure. Physical methods such as using optical energy, thermal energy or mechanical vibration energy as stimuli to the biomaterial have not been studied in the current literature.

2.5.3 State of the knowledge of chitosan degradation

Chitosan degradation follows the same mechanism as discussed before (see Section 2.5.2), in particular at the structural level molecular chains break down and so do chemical bonds. The first action will produce debris and the second action will produce monomers of N-acetyl-D-glucosamine unit and deacetyl-D-glucosamine unit (Kumar *et al.,* 2004). The following factors have significant influences over chitosan degradation.

Degradation of chitosan could be accelerated by means of irradiation, pH, temperature, and enzyme (Kumar *et al*., 2004). In particular, Tsaih and Chen (2005) reported that chitosan can be degraded by radiations, such as ultrasonic, ultraviolet and gamma. They discovered that the molecular weight of chitosan solution decreased significantly and that exposure time played an important role in this approach. There was a report to regulate pH to influence **c**hitosan degradation (Vårum *et al.*, 1997); in particular, chitosan is found to be dissolved in an acid solution with pH under 6.5.

Chitosan can be decomposed under 200°C. This temperature is low compared to those for other biopolymers (Pawlak & Mucha, 2002). Degradation behavior of chitosan was studied in the temperature range of 100-450°C by Pawlak & Mucha (2002). In particular, they produced thermo-gravimetric (TG) measurements in dynamic conditions for the aforementioned temperature range, where temperature changes at a constant rate of 15°C/min; see Fig. 2.7. However, information regarding degradation of chitosan below 100°C was not readily available in the current literature.

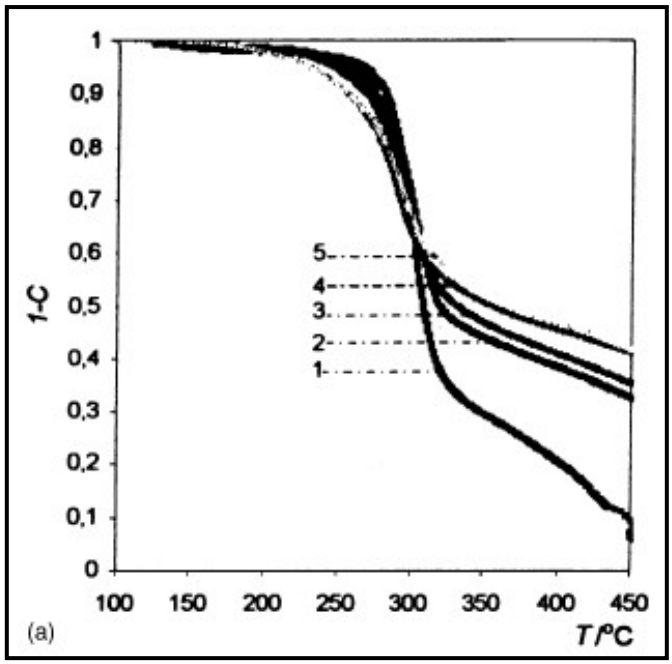

Figure 2.7. The thermo-gravimetric (TG) curves obtained for CH/S system. Curves from 1 to 5 represent various weight fractions of chitosan, which are as follows: (1) 1; (2) 0.8; (3) 0.6; (4) 0.2; (5) 0. C in the vertical axis denotes conversion degree which represents the ratio between degraded chitosan and the initial chitosan amount (Pawlak & Mucha, 2002).

Chitosan can be hydrolyzed by enzymes, e.g., lysozyme (Salton, 1952). Lysozyme hydrolyses β-(1-4) glycosidic linkages, and its natural substrate is of certain bacterial

cell wall peptidoglycans (Maeda *et al*., 1997). The hydrolysis process induced by lysozyme follows the Michaelis-Menten model. The model describes the rate of irreversible enzymatic reaction by relating the reaction rate to the concentration of the substrate (Vårum *et al.*, 1997). However, these studies only concerned the so-called homogeneous system where there is only one phase of materials. The heterogeneous system (where substrate is not soluble in solid phase) has recently become of interest, as it is closer to the real situation (Sikorski *et al.*, 2005). Correspondingly, modeling of chitosan in the heterogeneous system has not been reported in literature.

2.5.4 Modeling of biomaterial degradation

The goal of modeling degradation is to establish a mathematical expression of degradation rate, a particular biomaterial, and various factors. There are generally three ways to establish such a model (Petersen *et al.*, 2010): phenomenological, probabilistic, and empirical.

Phenomenological models are developed based on the governing equations including reaction, diffusion, and dissolution. They are applicable to a wide variety of polymer types, device geometries and conditions. However, they are specific to a certain system. In many cases, it is non-trivial to get solutions for these equations. Early models of this kind were ones developed by Thombre and Himmelstein (1984; 1985). For more recent models refer to Antheunis *et al*. (Antheunis *et al*., 2010).

This modeling approach is widely used for bulk degradation capturing complex reaction behavior as well as a mixed bulk and surface degradation process which involves both micro and macro scales. A recent model proposes i-1 possible degradation reactions for a polymer chain of average length with i monomers. The model takes into account of the effect of polydispersity in the micro-scale process of chain scission and in the meantime considers the effect of chain size on polymer diffusivity (Soares & Zunino, 2010). An example of modeling at macro-scale is the model developed by Lao *et al*. (2008), which models the degradation process of polymer blends. The model used information of degradation characteristics of two polymers (PLGA and Polycaprolactone (PCL)) in the application of predicting drug release.

Probabilistic models are developed by applying probability distributions of kinetics of molecules, which is in particular related to diffusion mass transfer and chemical reaction which are basic mechanisms underlying the degradation. Monte Carlo techniques are commonly used (Siepmann & Göpferich, 2001). For instance, Zygurakis (1996) used the Monte Carlo (MC) technique to model degradation and erosion first; however, the model did not consider the effects of diffusion. Göpferich (1997) combined the probabilistic MC approach with a phenomenological model which accounts for erosion. Such a kind of model can also be used to calculate degradation time by a random assumption. Siepmann *et al*. (2002) modeled polymer

degradation using the MC technique similar to the one used by Göpferich (1997), and they demonstrated the possibility to calculate degradation time with the assumption that the degradation is a random process (Fig. 2.8). The probabilistic approach was also used to model porosity (Rothstein *et al*., 2008). The model accounted for the observed drug release kinetics from polymer matrices by pores growth. The porosity used in their model is shown in Equation (2-2).

$$\varepsilon(t) = \frac{1}{2}\left[erf\left(\frac{t-\bar{\tau}}{\sqrt{2\sigma^2}}\right) + 1\right] \quad (2\text{-}2)$$

where, $\bar{\tau}$ and σ^2 are the mean and variance. This model illustrated the relationship between the initial burst and the drug located inside the device surface. However, the model is limited in that it requires specification of pore formation which is a difficult task.

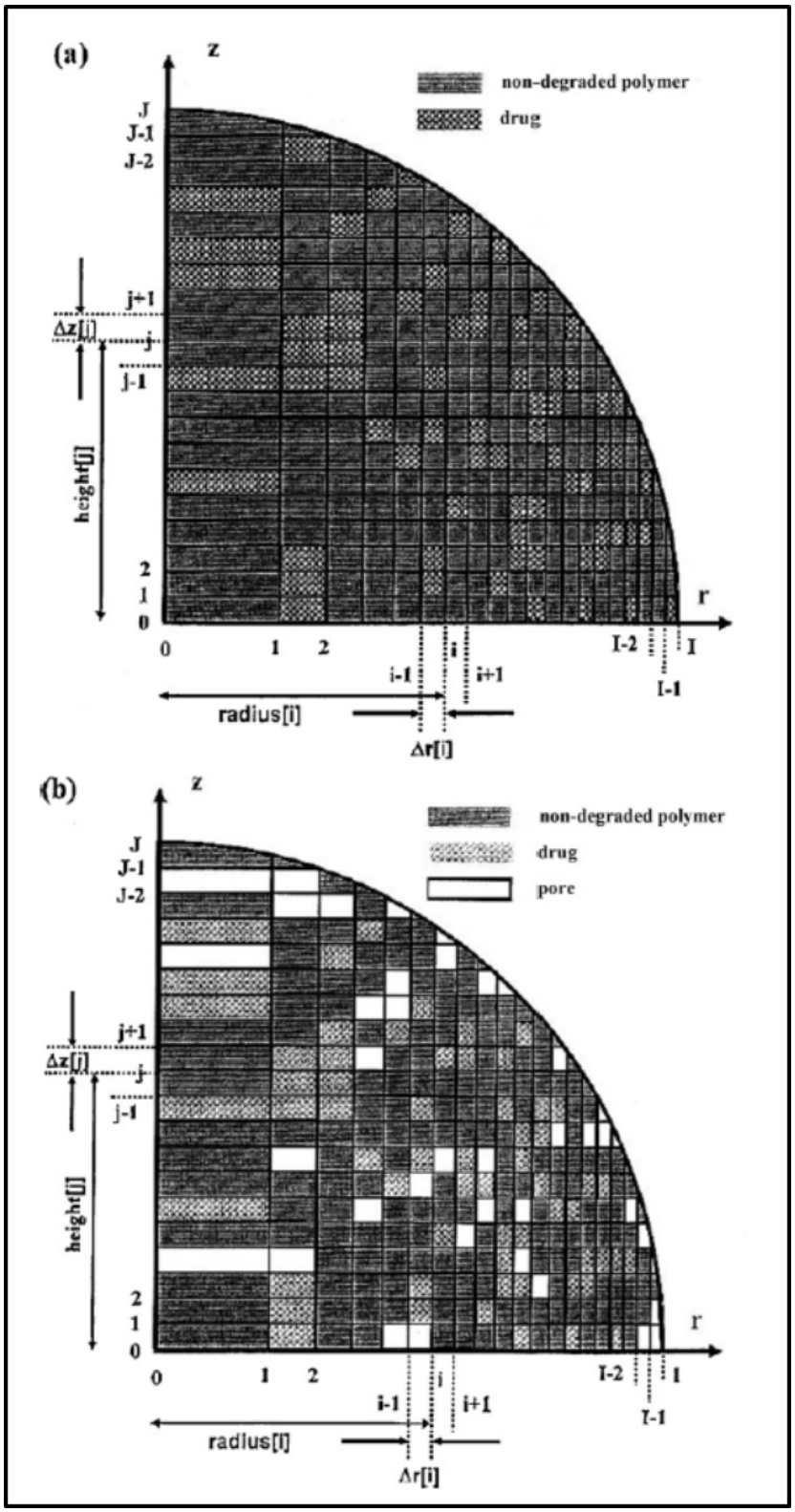

Figure 2.8. Monte Carlo approach to modeling polymer degradation: (a) before degradation; (b) after degradation (Siepmann *et al*., 2002).

Empirical models are developed based on some test information by regression techniques in general. The test information is gathered through controlled experiments. The earliest model of this kind may refer to Höpfenberg & Hsu (Höpfenberg & Hsu, 1978). In developing such a kind of model, some heuristic knowledge may be used; see the work of Lao *et al*. (Lao *et al*., 2008). One of the advantages with this approach is that significance of a particular factor can be discerned. For instance, Li *et al*. (2011) fitted polyanhydride copolymers degradation with two exponential functions that contained five parameters. The two parameters are the most important factor according to their analysis.

One of the important limitations with empirical models is the validity of the test-bed. Most degradable polymers are not water-soluble. Test-beds are essentially organic solvent-water mixtures, and the test-beds involve many complex effects. For instance, degradation of water-soluble oligomers could be in equilibrium with the formation of oligomers from monomers in aqueous solutions.

2.5.5 Biosensors related to degradation control

There is no biosensor available in the current literature regarding real-time measurement of degradation rate of scaffold in tissue regeneration. However, there are developments of sensors that are potentially relevant to biosensors for real-time measurement of degradation rate of tissue scaffolds. These sensors are mostly built

upon carbon nanotube (see Appendix D for details of carbon nanotube) (Stegemann *et al*., 2008). One class of the CNT-based sensors is made by mixing up CNT and polymers to form a conductive film. Such a film sensor has found its applications in monitoring of pulse rate, temperature (Wilson & Gifford, 2005), blood glucose (Hu *et al.*, 2010), detection of pH value (Wilson & Baietto, 2011), monitoring of total cholesterol in blood, and diagnosis of diseases as specific DNA sequences (Shung *et al*., 2011).

2.6 Conclusion

From the above discussion, it is now clear that the state of the art of degradation control in the application of tissue scaffolds is such that there are two schools of ideas, concepts and techniques: Scaffold material modification and cell culture environment adjustment. The latter stops functioning when the scaffold is put in human body. The two schools are of an open-loop control strategy, which is very sensitive to disturbances and noises.

The proposed research in this thesis, defined in Chapter 1, is based on the idea of a close-loop control strategy for degradation rate control in the application of tissue scaffolds, which has never been studied in literature. Regarding the first objective of this research, there has been no work in the current literature on understanding a joint thermal and enzymatic effect. In other words, the existing work did generate fruitful

results on thermal effect but without consideration of the influence of enzymes. The second objective is unique in that thermal and enzymatic effects are jointly considered. The third objective is new in the application of tissue scaffolds.

CHAPTER 3

THERMAL AND THERMAL-ENZYMATIC EFFECT ON DEGRADATION

3.1 Introduction

To gain a better understanding of chitosan degradation behavior under the effect of temperature and enzyme, this chapter studies the thermal effect, enzyme effect, and conjoint enzymatic-thermal effect on chitosan film degradation. It is noted that the enzymatic effect on chitosan degradation has already been well known (Freier *et al*., 2005), so this effect was not studied. In this study, there were two hypothesises. Hypothesis I: there is a significant effect on chitosan film degradation by means of temperature regulation in the temperature range from 37°C to 50°C. Hypothesis II: there is a significant effect on chitosan film degradation by means of simultaneously regulating temperature and using different enzymes. Accordingly, two experiments were designed and conducted.

3.2 Materials and Method

3.2.1 Design of the experiments

In Experiment I (thermal effect), a full factorial experiment with two factors was employed. The two factors are: temperature and time. Each factor has two levels; thus

the whole experiment has 4 runs in total. The levels of the factors are shown in Table 3.1. The experiment set two groups corresponding to the two levels of temperature treatment: group A (37˚C) and group B (50˚C). Each run contains 5 samples (chitosan films). The dry weight of the chitosan film was measured in two different times: at the beginning or the first day and on the 28^{th} day. The full factorial runs are shown in Table 3.2.

Table 3.1. Levels of each factor in Experiment I (thermal effect).

The 2 levels of each factor		
Factor	Levels	
	Level 1 (coded -1)	Level 2 (coded +1)
Temperature	37°C	50°C
Time	1 day	28 day

Table 3.2. Scenario of 2 factors full factorial design in Experiment I (thermal effect).

Temperature		-1	1
Time	-1	Group A (I)	Group B (I)
	1	Group A (II)	Group B (II)
The code is represented in Table 3.1			

In Experiment II (conjoint thermal-enzymatic effect), an assumption was made in this experiment: time and enzyme has no interaction. This assumption implies that the activity of lysozyme is a constant during degradation process. An experiment with 3 factors and 2 levels for each factor was designed. Table 3.3 summarizes the 2 levels of each factor.

Table 3.3. Levels of each factor in Experiment II (conjoint thermal-enzymatic effect).

The 2 levels of each factor		
Factor	Levels	
	Level 1 (coded -1)	Level 2 (coded +1)
Enzyme	zero	50,000 U/mL
Temperature	37°C	50°C
Time	0 day	72 hours

The experiment scenario is further shown in Table 3.4. Four groups were set: groups A, B, C, and D. Groups A and B are for the temperature 37ºC, and Groups C and D are for the temperature 50ºC. As shown in Table 3.4, samples in group A were settled in Phosphate buffered saline (PBS) solution without lysozyme and at 37°C; samples in group B were settled in PBS solution with lysozyme and at 37°C; samples in group C were soaked in PBS solution without lysozyme and at 50°C; and samples in group D were soaked in PBS solution with lysozyme and at 50°C. Further in Table 3.4, mark "I" denotes the first hour and mark "II" denotes the 72nd hour.

Table 3.4. Scenario of 3 factors full factorial design in Experiment II (conjoint thermal-enzymatic effect).

Temperature		-1		1	
Lysozyme		-1	1	-1	1
Time	-1	Group A (I)	Group B (I)	Group C (I)	Group D (I)
	1	Group A (II)	Group B (II)	Group C (II)	Group D (II)
The code is represented in Table 3.3					

3.2.2 Material

Chitosan was used as received. Its molar mass is approximately 700,000 g/mol. The DD was 60%. Ethanol was purchased from Sigma-Aldrich Canada Ltd. (Oakville, ON, Canada). The 3% acetic acid was prepared using 99% aqueous acetic acid and distilled water. Lysozyme from chicken egg white (Sigma L-6878, Grade I) was used as received. Lysozyme solutions of 50,000 U/mL were prepared by dissolving Human lysozyme (recombinant DNA molecules expressed from rice) with 100,000 U/mg in distilled water. Phosphate buffer saline (PBS) solution was prepared by a standard process. All the chemicals and solvents used in experiments were purchased from Sigma-Aldrich Canada Ltd. (Oakville, ON, Canada).

3.2.3 Chitosan film preparation

The 4 g chitosan powder was dissolved in 100 mL 3% acetic acid. The solution was stirred at 37˚C at 350 r/min by hotplate for 3 hours until chitosan is completely dissolved in acetic acid. Chitosan solution was processed by Allegra X-22R centrifuge at 37°C at 2000 r/min for 10 min. Chitosan solution was added into 24 well petri dish and then made the solution to each well by 200 µL. The petri dish which contained the chitosan solution was put into an oven for 7 hours at 60˚C to induce water evaporation from solution. After 7 hours period, the dry chitosan films were obtained.

Then diluted 10% ethanol into petri dish (5 μL/well) and the ethanol was allowed to dry at room temperature.

The 1% NaOH solution was used for washing the chitosan films by putting the film into the prepared NaOH solution and stirring them at 350 r/ min for 30 min. The film was then put on a glass board and dried for 7 hours at 60˚C. The washing process was repeated three times for each film. The produced chitosan film is shown in Fig. 3.1.

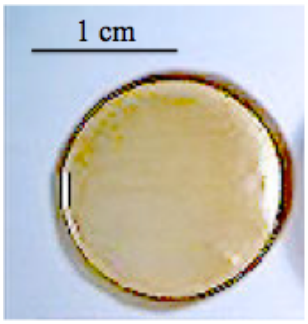

Figure 3.1. Chitosan film.

In Experiment I, the *in-vitro* degradation of chitosan processed in 1 mL phosphate-buffered solution (PBS, pH 7.4) at 37°C and 50°C. The PBS solution was refreshed daily to ensure pH of solution. After the 4 weeks' degradation process, samples were removed from the medium, rinsed with dd water (double-distilled water), dried and finally weighed. The degraded amount was represented as percentage of mass loss of the dried films. There are in total 5 samples in each group.

In Experiment II, similar processes were followed. However, both solution and time span were made different from the aforementioned one. Here, chitosan films were followed by putting them in 1 mL phosphate buffered saline solution (PBS, pH 7.4) with or without 50,000 U/mL lysozyme. The concentration of lysozyme was chosen to correspond to the concentration in human serum. The lysozyme solution was refreshed daily to ensure continuous enzyme activity. After 72 hours, samples were removed from the medium, rinsed with dd water, dried, and finally weighed.

3.2.4 Fourier transform infrared spectroscopy (FT-IR) spectrum

The structural information of the films was confirmed from FT-IR analysis. Chitosan film samples were measured in Exmperiment I at the 0 day and the 14th day after degradation experiments, respectively, in order to confirm the integrity of the films. The '0 day' refers to a time period of 3 - 4 min after soaking chitosan films into PBS solution. That definition of the 0 day is applied throughout the whole thesis.

3.2.5 Mass loss measurement

Degradation of chitosan film was represented by mass loss (dry), which was calculated by the following equation:

$$\text{Mass Loss} = \frac{W_0 - W_t}{W_t} \times 100\% \quad (3\text{-}1)$$

In the above equation, W_0 is the initial dry weight of a chitosan film; W_t is the dry weight of the chitosan film after degradation. Further, W_0 was measured after drying chitosan films to a temperature near but below 60°C; W_t was measured by the same drying operation.

3.3 Results and Discussion

3.3.1 FT-IR spectrum

Fig. 3.2 shows the FT-IR spectra of the sample at the initial time (0 day), the sample after the 14 days with temperature of 37°C and the sample after 14 days with temperature of 50°C, respectively. From Fig. 3.2, the peak pointed by red arrow (long dash line) is the peak of -O-C-O- bond; the peak pointed by yellow arrow (short dash line) is the data related to D-glucosamine unit; and the peak pointed by blue arrow (solid line) is the data related to acety-D-glucosamine unit. These function groups are the chemical representation of chitosan. This result implies that the chitosan films keep a good integrity for all the stages in the experiment.

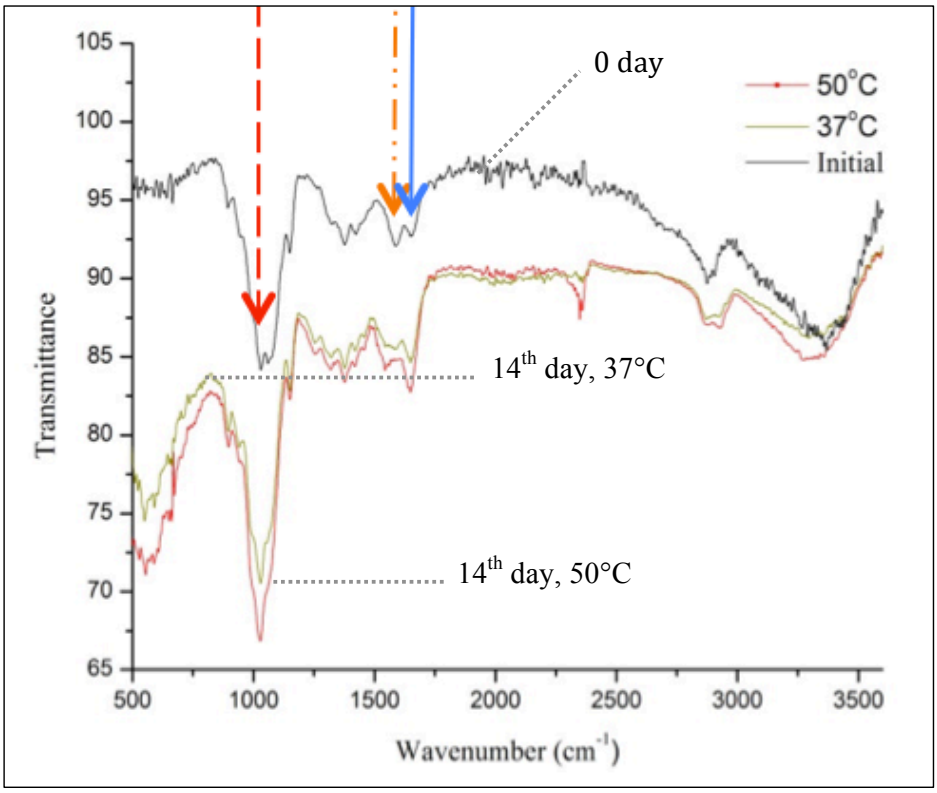

Figure 3.2. FT-IR spectra of chitosan at 0 day and the 14th day. Black line (top): FT-IR spectra of Group A and B (two lines overlapped); Green line (middle): FT-IR spectra of Group A at the 14th day; Red line (bottom): FT-IR spectra of Group B at the 14th day.

3.3.2 Experiment I

The result of degradation in terms of mass loss of chitosan films is summarized in Fig. 3.3. An increased mass loss was observed for films under higher temperature after 28 days. In particular, mass loss of the samples in Group B was up to 10% after 28 days. In contrast, mass loss of the samples in Group A after 28 days is 4%. It is noted that

according to t-test, all these changes are significant. No sample gained large degradation (over 50%) in the period considered in the experiment.

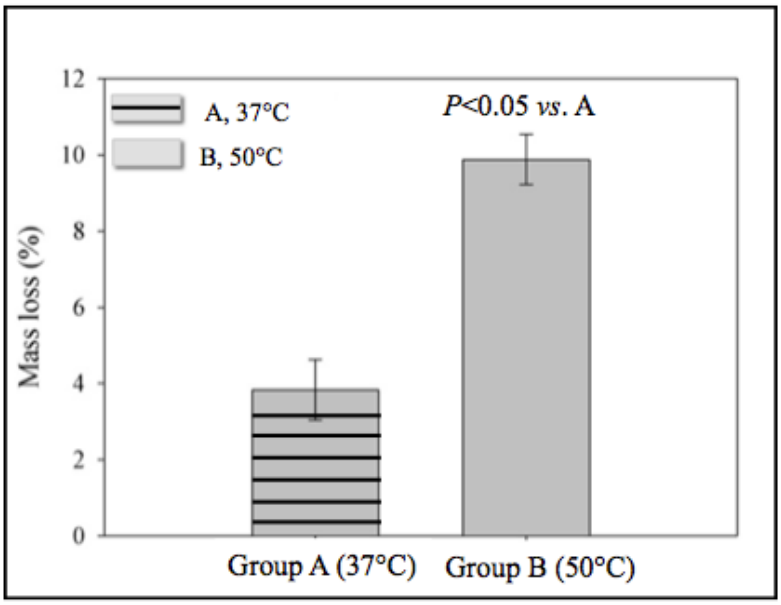

Figure 3.3. Mass loss of chitosan films in Group A (37°C) and Group B (50°C) are shown as mean ± standard deviation (n=5). Mass loss was analyzed by paired-sample t-test (t=-13.598, P<0.05). Output is shown in Appendix E.

The mass loss of chitosan films in this experiment may be attributed to breakages of molecular chains. When temperature is sufficiently high, Brownian motion of molecules both in solution and chitosan films increase as they have gained more energy. Thus, the crash between water molecules and molecular chains of chitosan increases both in frequency and intensity. This can further accelerate the breakage of molecular chains.

The dry weight of chitosan films was analyzed by the Repeated-Factor (RF) method in statistics. The main effect of temperature and time, respectively, and interaction between time and temperature were analyzed by type III method. Further SPSS software was employed to perform this analysis. Detailed results are put in Appendix E. A summary of the results is presented below.

Fig. 3.4 shows the main effect and interaction effect, where a care must be taken that the lines in this figure do not make sense of any linearity between independent variable and dependent variable but are of convesion in factorial analysis in statistics. Note that the dry weight in Fig. 3.4 (a) is ccalculated by averaging the dry weights at temperature of 37°C and 50°C. Fig. 3.4(a) and (b) show that both time and temperature can affect degradation of chitosan film. Longer time span or higher temperature can induce mass loss in chitosan films. Further, in Fig. 3.4(a), dry weight decreases by 1 mg; while in Fig. 3.4(b), dry weight decreases by 0.5 mg. Fig. 3.4(c) shows that there is an interaction effect between temperature and time. In particular, two lines start from the same point in Fig. 3.4(c); however, line B decreases faster than line A thereafter. This implies that temperature has more influence over time.

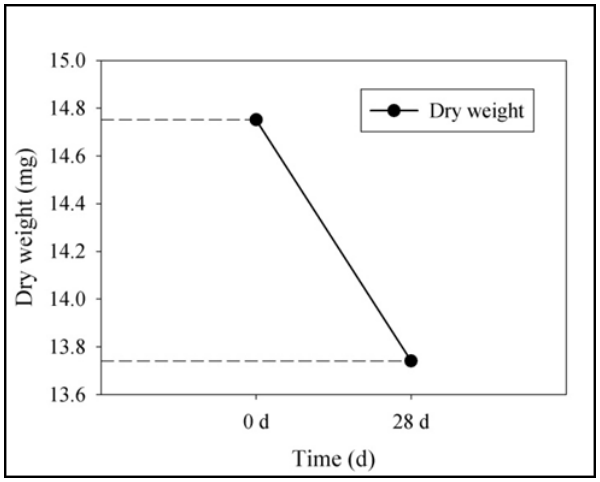

(a) Main effect of time

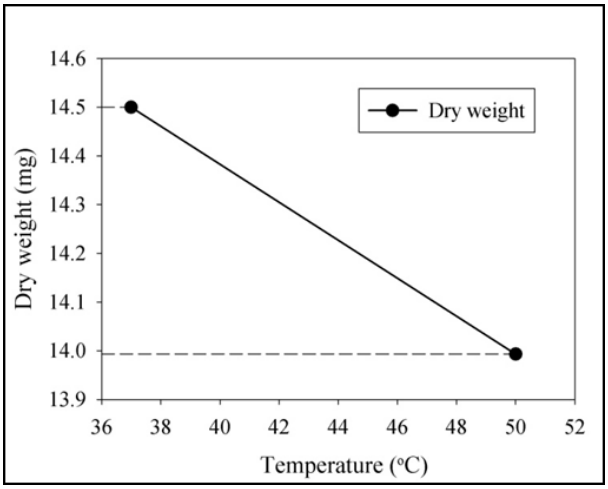

(b) Main effect of temperature

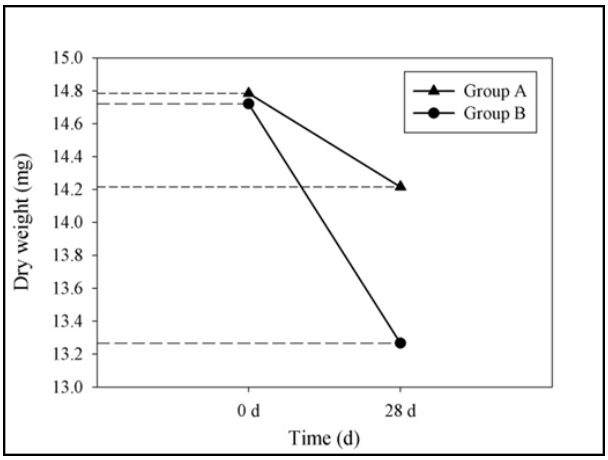

(c) Interaction effect

Figure 3.4. Main effect and interaction. (a) main effect of time; (b) main effect of temperature; (c) interaction between time and temperature.

3.3.3 Experiment II

Fig. 3.5 shows the results Experiment II. The results in Fig. 3.5(a) and Fig. 3.5(b) show a similar trend as that in Fig. 3.3, which implies the thermal effect at play. In particular, mass loss in a lower temperature group was smaller than that in a higher temperature group. However, the degradation behaviors between the two temperature groups are quite different (0.2% difference in Fig. 3.5(a), while 42% in Fig. 3.5(b))

Further, the environment of the experiment in Fig. 3.5(a) was similar as that of Experiment I (i.e., thermal effect experiment). In Fig. 3.5(b), lysozyme is in the PBS solution. The large difference in degradation of the samples in Fig. 3.5(a) and Fig. 3.5(b) clearly suggests that temperature affect enzymatic hydrolysis significantly. In fact, the degradation rate of the samples, as shown in Fig. 3.5(a), is only 1% (which can certainly be ignored in tissue engineering applications). In contrast, mass loss of the samples in group B and group D are up to 80% within 72 h of degradation (Fig. 3.5(b)). Degradation of the chitosan films in group D (50ºC) was two times faster than that in group B (37ºC). Compare Fig. 3.5(a) with Fig. 3.5(b), an increased mass loss was observed for films in lysozyme solution than PBS, which can also be represented by Fig. 3.5(c).

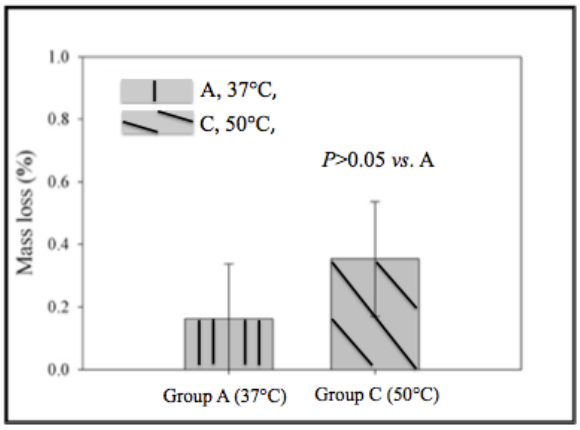

(a)

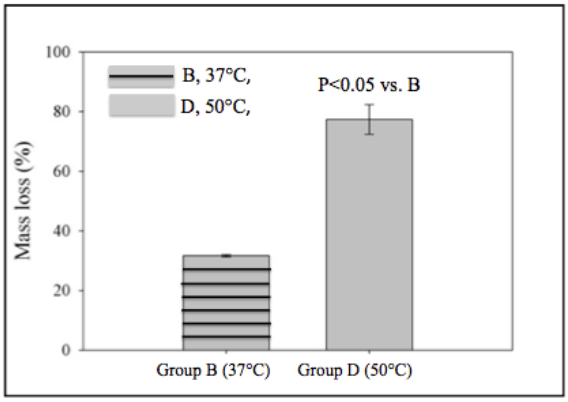

(b)

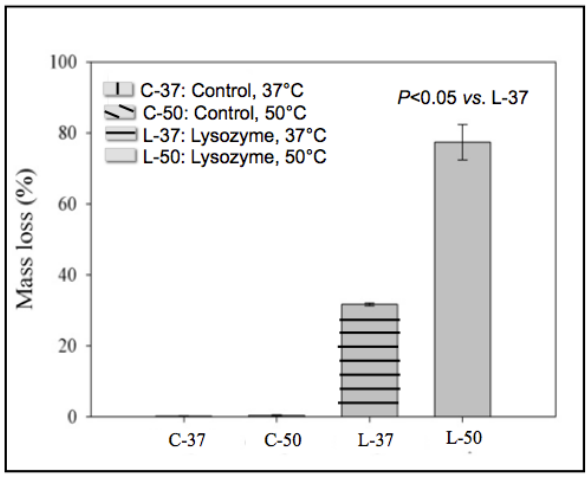

(c)

Figure 3.5. Mass loss of chitosan films in different groups. (a) Mass loss of control groups; (b) mass loss of lysozyme group; (c) mass loss of the four groups. Data are shown as mean ± standard deviation (n=5). Mass loss in (a) and (b) was analyzed by paired-sample t-test: (a) t=3.56, P>0.05; (b) t=14.78, P<0.05. Complete data are shown in Appendix F.

One important finding here is that the enzymatic effect seems to be more active than thermal effect under 50°C. It is well known that enzyme plays a catalytic role during hydrolysis. In this experiment, chemical chains are hydrolyzed into monomers directly. Thus, mass loss induced from enzymatic hydrolysis is larger than thermal decomposition at 50°C.

The dry weight of chitosan films was further analyzed by the Repeated-Factor (RF) method. The interaction between temperature and time, the interaction between temperature and enzyme and the interaction among time, temperature and enzyme were analyzed by type III method (in particular). Completed data analysis are shown in Appendix F.

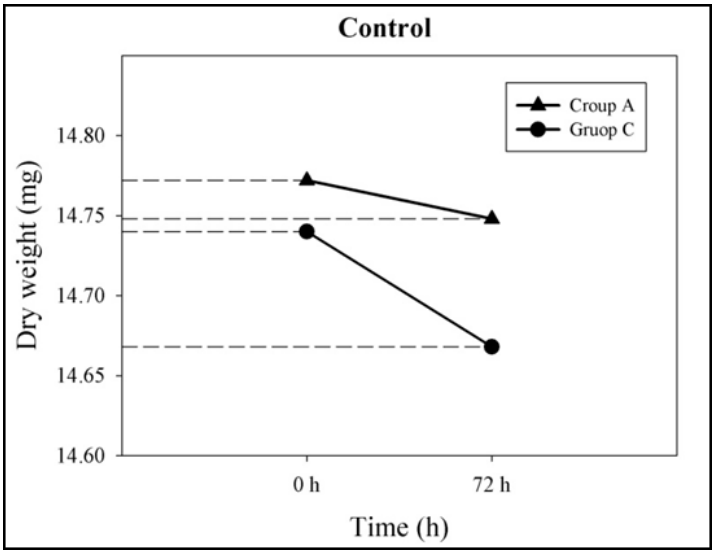

(a)

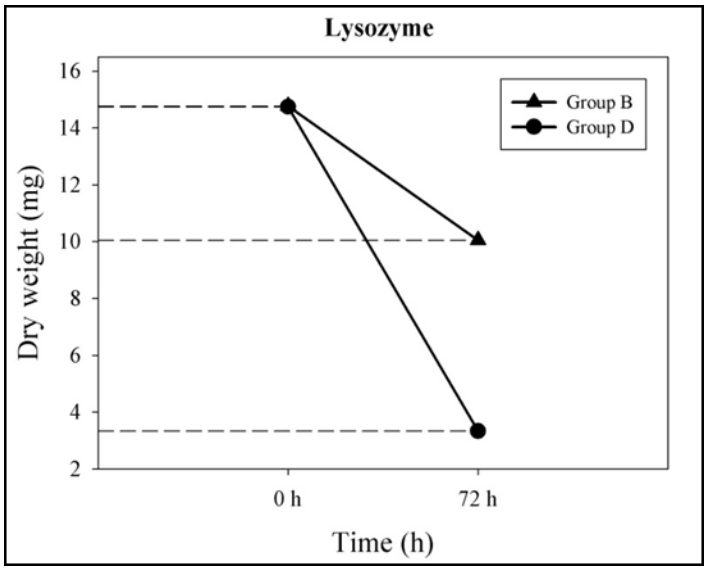

(b)

Figure 3.6. Two factor interaction between temperature and time under two different enzyme levels. (a) The interaction between temperature and time in control groups; (b) the interaction between temperature and time in lysozyme groups.

The interactions between temperature and time under two different enzyme levels are shown in Fig. 3.6. From Fig. 3.6(a) and Fig. 3.6(b), it can be seen that the slopes of

line B and line D are steeper than those of line A and line C in Fig. 3.6(a). Dry weight loss in lysozyme solution is larger than PBS solution under different temperatures.

The interactions between temperature and enzyme under two different time levels are shown in Fig. 3.7. Fig. 3.7(a) shows that temperature and enzyme have interaction at initial time, though the interaction was not significant. Fig. 3.7(b) shows a similar trend. The three factor interation are shown in Fig. 3.8.

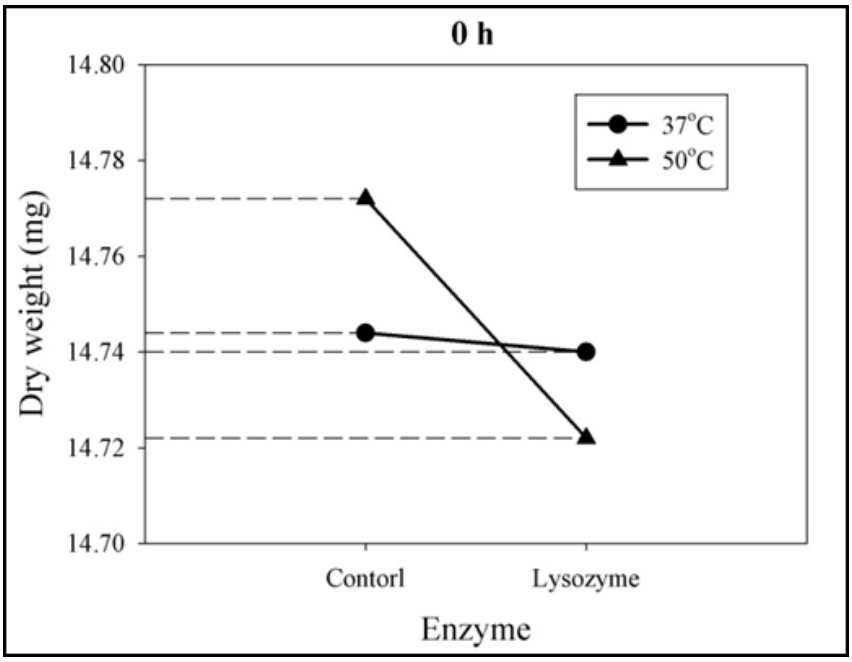

(a)

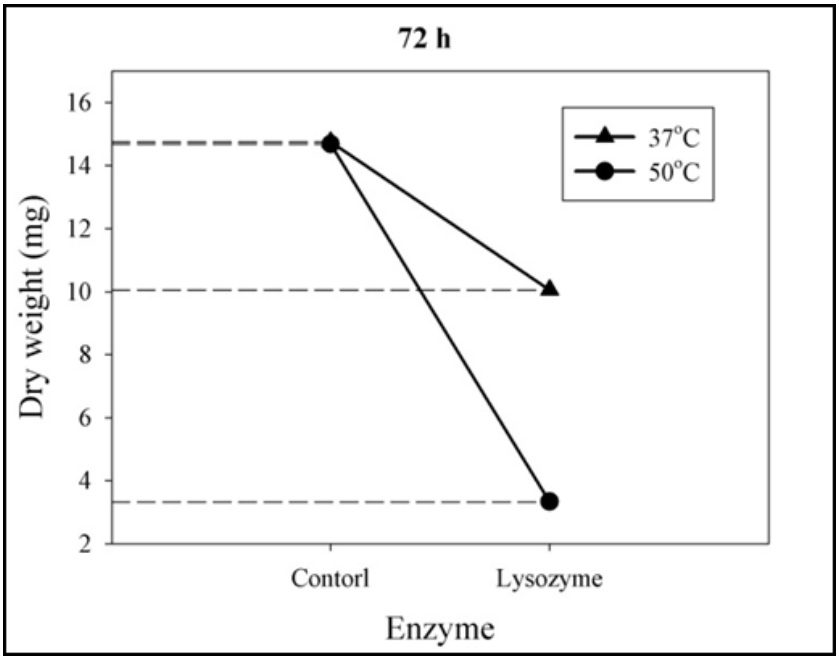

(b)

Figure 3.7. Interaction between temperature and enzyme under two different time levels. (a) Interaction between temperature and enzyme after 0h; (b) interaction between temperature and enzyme after 72h.

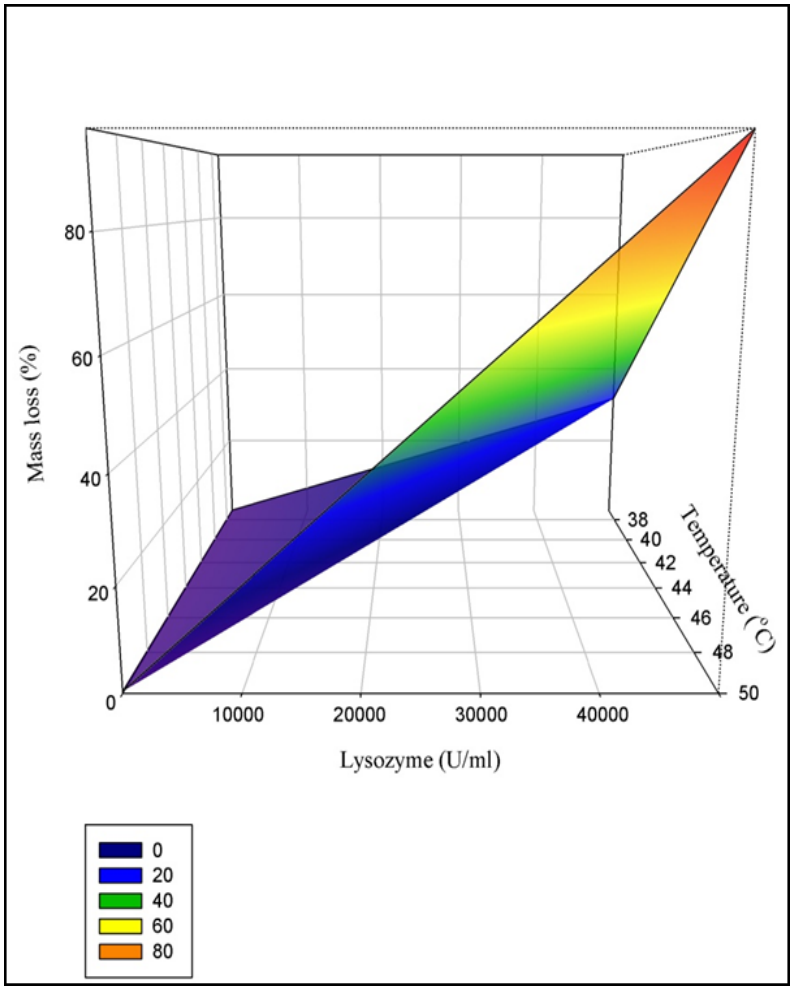

Figure 3.8. Interaction of temperature, enzyme and time.

According to the thermal property of lysozyme, its activity will increase at higher temperature. However, the upper limit should be lower than 60°C. Otherwise, lysozyme will be denatured. In this experiment, lysozyme shows its temperature-dependent potential. At 50°C, the mass loss of chitosan films is two times that at 37°C. That maybe due to the increased activity of electron transformation under higher temperature. At 50°C, electron in lysozyme can be transformed much faster than at 37°C; thereby enzymatic hydrolysis rate can be increased. Thus, chitosan degradation rate increased faster in lysozyme solution.

3.4 Conclusions with Further Discussion

The following conclusions can be drawn from the results obtained:

(1) Temperature is an important factor which influences degradation of chitosan. The higher temperature will lead to faster degradation. However, this factor is not significant when temperature is under 50˚C.

(2) The higher temperature, in particular in the experimental condition (37°C to 50°C), can accelerate lysozyme hydrolysis activities and thus accelerate degradation rate of chitosan films.

(3) Three factor interactions among temperature, enzyme and time have larger effect than the two factor interaction temperature-enzyme on chitosan film degradation.

(4) Temperature, enzyme and time can be used together as control factors for chitosan-based scaffold degradation control in tissue engineering.

The thermal degradation has been studied in the current literature. However, most of the sutdies were performed under accelerated conditions with a high temperature range from 100°C to 300°C in a air-tight dry circumstance. To the auther's best knowledge, the *in-vitro* thermal degradation study below temperature 50°C has not been sudied in the current literature.

CHAPTER 4

MODELING OF DEGRADATION RATE OF CHITOSAN SCAFFOLDS

4.1 Introduction

In this chapter, modeling of degradation rate will be discussed. The goal of modeling was to develop a mathematical model with which to predict degradation rate with time, temperature, enzyme as three independent variables. Degradation rate is represented by mass loss over a period of time. Such a model is as important as a so-called plant dynamic model in the general control system.

One of the novel ideas in developing the aforementioned model was to establish a layer-by-layer 3D structure model for chitosan scaffold to simulate the bulk degradation by incorporating both thermal and enzymatic effects. Another novel idea was to incorporate the conjoint thermal and enzymatic effect in degradation rate. Overall, the model was developed by a combined empirical-based and principle-based approach. In particular, an empirical-based approach was applied to develop the conjoint thermal and enzymatic effect, and a principle-based approach follows a stochastic process which was applied to the molecule-level acitivity of degradation.

The remaining part of this chapter is organized as follows. Section 4.2 presents data collection along with the corresponding experiment, which was used to develop the

conjoint thermal and enzymatic effect. Section 4.3 presents the model development. Section 4.4 provides validation of the model. Section 4.5 gives a conclusion with discussion.

4.2 Modeling of the Conjoint Thermal and Enzymatic Effect

An empirical-based approach was employed to develop a model, which takes into account the thermal and enzymatic conjoint effect. The first step was to develop the relationship among enzymatic activity and temperature. The second step was to formulate a model for degradation – mass loss in this case. This section will fulfill the first step, and the second step will be discussed later in Section 4.3. It is noted that lysozyme was used in this study.

4.2.1 Materials

Chitosan with a molar mass of approximately 400,000 g/mol was purchased from Fluka (Oakville, ON, Canada) and was used as received. Human lysozyme, purchased from Sinma-Aldrich (Oakville, ON, Canada) (recombinant DNA molecules expressed from rice) with 100,000 U/mg was used as received. *Micrococus lysodeikticus* was purchased from Sigma-Aldrich (Oalville, Canada) and was used as lysozyme substrate. Reaction buffer was prepared using 50 mL of 0.1 M sodium phosphate, 0.1 M sodinm chloride, pH 7.5, containing 2 mM sodium azide as a preservative to avoid

the buffer to be ruined. All the other chemicals were purchased from Sigma-Aldrich (Oakville, ON, Canada) and used as received.

4.2.2 Methods

4.2.2.1 Measurement of lysozyme activity

The general idea to prescribe two independent variables (temperature and lysozyme) was to prepare samples that contained lysozyme under different temperatures. The samples were then measured for their luminescence with Luminance Microplate Reader. Lysozyme solutions ranging from 5000 U/mL to 500,000 U/mL were prepared as standards. This was completed by the following steps (Freier *et al*., 2005).

Step 1: Prepared lysozyme substrate suspension and lysozyme solution. Prepared a 1.0 mg/mL lysozyme substrate suspension by putting 1 mg lysoyzyme substrate (*micrococcus lysodeikticus*) suspension into 1 mL of dd water. Dissolved the lysozyme in 1 mL of dH_2O to prepare lysozyme solution with 100,000 U/mL.

Step 2: Diluted the samples. Filled 3 wells of 96-well petri dish with 150 μL of reaction buffer (see section 4.2.1), so each well contained 50 μL of reaction buffer. Added 50 μL of lysozyme solution into each well, respectively. Thus, the lysozyme

activity concentration was 50,000 U/mL in each well. Filled 3 other wells with 50 µL of dH_2O as control groups.

Step 3: Began the reaction. Added 50 µL of the lysozyme substrate suspension (prepared in Step 1) to each well containing the lysozyme solution and dH_2O.

Step 4: Incubated the reaction mixture. Incubated the mixture for 10 minutes at certain temperatures (Table 4.1).

Step 5: Measured the luminescence of the lysozyme substrate by Luminance Microplate Reader (Fluoroskan Ascent, Thermo Labsystems, Finland) (Fig. 4.1) to capture the absorbance spectrum at 450 nm at the resolution of 1 nm.

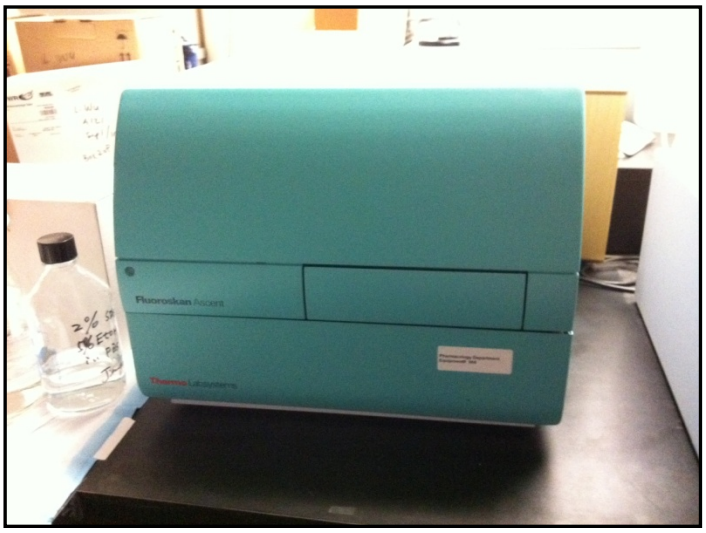

Figure 4.1. Luminance Microplate Reader.

Step 6: Corrected the background noise. Subtracted the value from the control sample (no-enzyme).

Step 7: Compared the result of luminescence with the standard curve to get the lysozyme activity at the temperatures specified in Table 4.1.

The above steps were repeated for different temperatures as listed in Table 4.1. In this way, the lysozyme activity at each temperature can be obtained. It is noted that the standard way to measure the lysozyme activity is obtaining a fluorescence-based assay (Nordtveit *et al*., 1994). However, in the present study, the concentration of lysozyme activity is sufficiently high, so the measurement of luminescence is possible.

Table 4.1. Temperatures used for enzyme activity measurement.

Temperature	25°C	30°C	34°C	37°C	45°C	50°C

4.2.2.2 Chitosan film fabrication

4 g chitosan powder was dissolved in 100 mL 3% acetic acid. The solution was stirred at 37˚C at 350 r/min by hotplate for 3 hours until chitosan was completely dissolved in acetic acid. Chitosan solution was processed by Allegra X-22R centrifuge at 37°C at 2000 r/min for 10 min. Chitosan solution was diluted into 24 well petri dish and

then made the solution to each well by 200 μL. The petri dish which contained the chitosan solution was put into an oven for 7 hours at 60˚C to induce water evapouration from solution. After 7 hours, the dry chitosan films were obtained. Then 10% ethanol was put into petri dish (5 μL/well) and the ethanol was left at room temperature until dried.

The 1% NaOH solution was used for washing the chitosan films by putting the film into the prepared NaOH solution and stirring them at 350 r/ min for 30 min. The film was then put on a glass board and dried for 7 hours at 60˚C. The washing process was repeated three times for each film.

4.2.2.3 The experiment of *in-vitro* hydrolysis of chitosan scaffold

The experiment of in-vitro hydrolysis of chitosan scaffold was about measurement of mass loss of a particular scaffold made of chitosan with respect to time. The purpose of this experiment was to validate a model of degradation of a chitosan scaffold, which will be discussed later in this chapter.

It followed in 1 ml phosphate buffer solution (PBS, pH 7.4) containing lysozyme 50,000 U/mL at 37°C. The concentration of lysozyme was chosen to correspond to the concentration in human serum. A total of 14 groups (5 films in each group) of chitosan films were settled in the lysozyme solution for 168 h (7 days). The lysozyme

solution was refreshed daily to ensure a continuous enzyme activity. The chitosan films were taken out every 12 hours, dried and weighed. After that, the mass loss of each group was calcualted from Equation (3-1).

4.2.3 Results and discussion

The relative activity of lysozyme (r) was obtained by dividing the lysozyme activity at an elevated temperature (i.e. the results of lysozyme activity measurement in Section 4.2.2.1) by the lysozyme activity at the temperature of 37°C. The relationship between the temperature and the relative activity of lysozyme at the initial time (in this study it was assumed that the enzymatic activity will keep unchanged in the duration of 12 hours) is shown in Fig. 4.2. The Y-axis represents the relative activity of lysozyme; X-axis denotes the temperature.

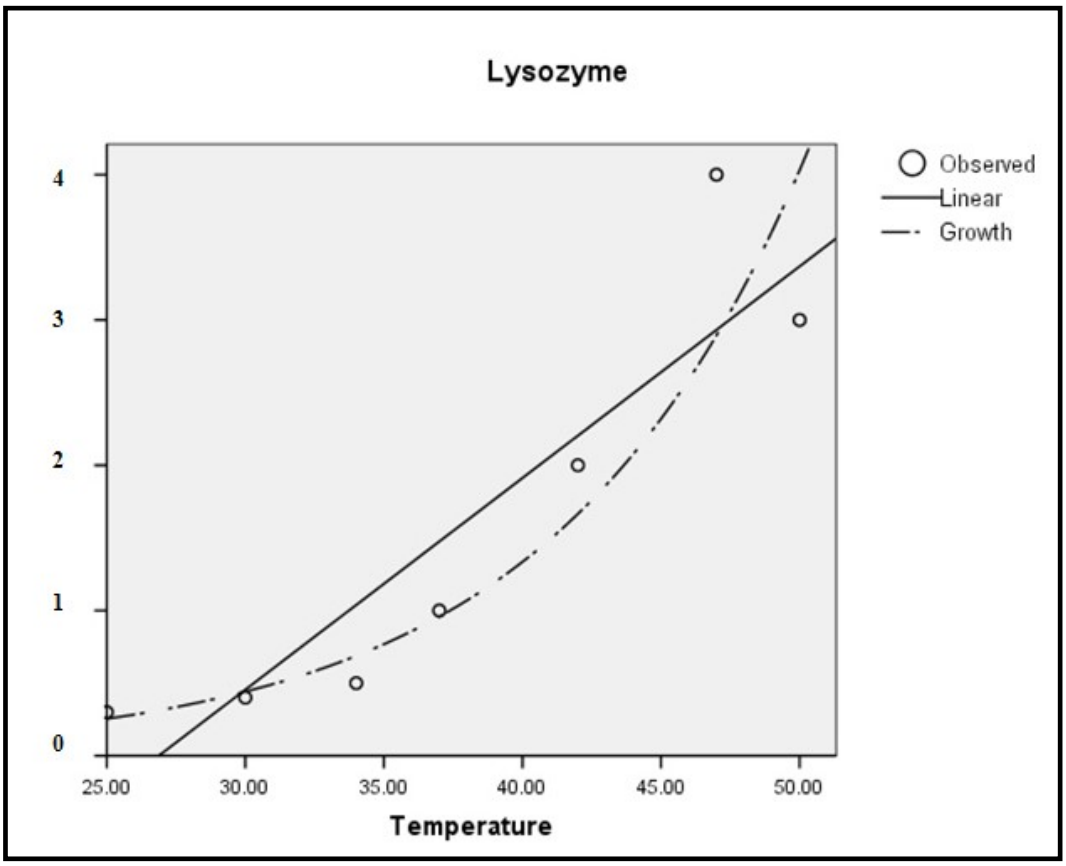

Figure 4.2. Relationship between temperature and lysozyme activity.

The relationship was further fitted in a Exponential Curve format with $R^2 = 0.942$ with SPSS, which is Equation (4-1). In this equation, *r* denotes the relative activity of lysozyme, and T denotes temperature (°C).

$$r(T) = 1.6e^{0.11T} \quad (4\text{-}1)$$

The detailed output of statistical analysis from SPSS can be seen in Appendix G.

4.3 Chitosan Degradation Model

There are several steps toward a model of degradation with consideration of both the thermal and enzymatic effects. The first step was to establish a 3D model with which to enable the description of degradation process. The second step was to define pixels based on the 3D models. The third step was to model the degradation of one pixel (in the 3D model) and then of the whole chitosan scaffold.

4.3.1 A 3D chitosan film model: chitosan scaffold model

The structure model of a chitosan scaffold is necessary to describe the degradation process of a chitosan scaffold. The chitosan scaffold studied in this thesis is viewed as consisting of a number of films (Fig. 4.3). Each film has a thickness. In this thesis, the thickness of film is 150 μm. With this model, a chitosan scaffold was considered as a cylinder. Let L denote cylinder height, and R denote cylinder radius. Then, in this study, it is assumed that $R \gg L \gg l_{\text{chitosan}}$, where l_{chitosan} is the length of a chitosan molecular chain.

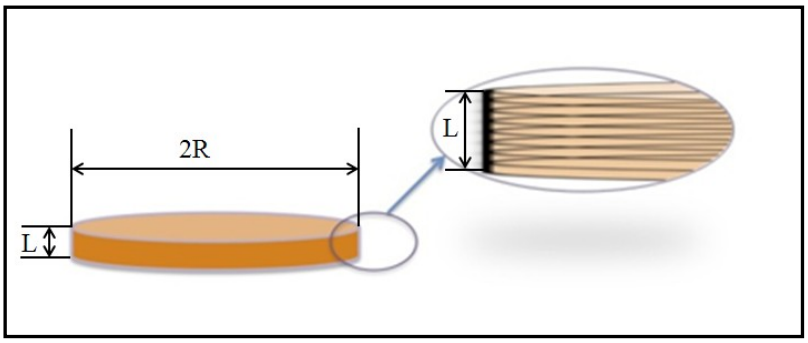

Figure 4.3. Chitosan film multi-layer model.

The schematic of the 3D model is further illustrated in Fig. 4.4(a). In the Z axis, chitosan scaffold film is divided into a number layers of films with the same length (Fig. 4.4(b)); in the XOY plane of each layer, the chitosan film is divided into *n* pixels (Fig. 4.4(c)). Each layer has the same number of pixels. The thickness of each layer is fixed. Thus, the total number of pixel is directly proportional to the total height of chitosan film structure model. The pixel was considered as basic degradation or erosion unit.

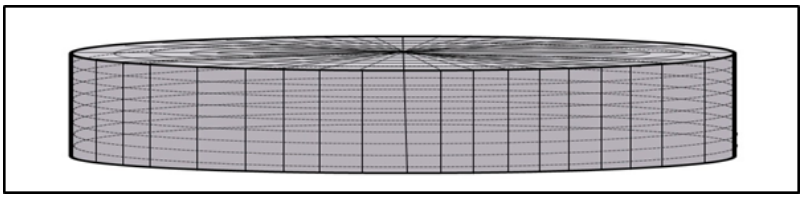

(a)

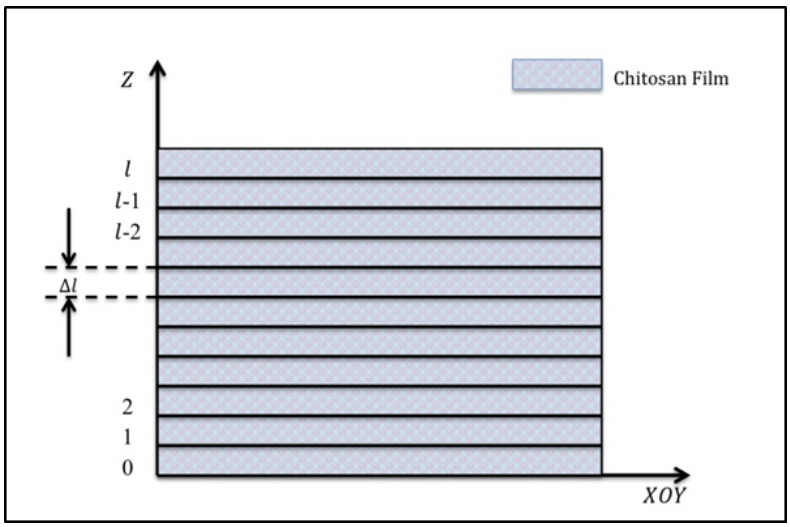

(b)

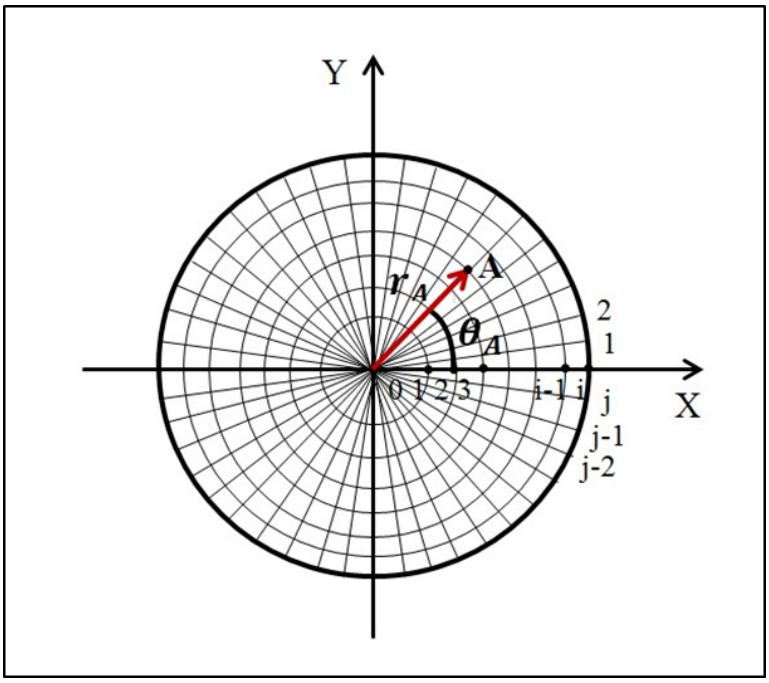

(c)

Figure 4.4. Chitosan Film Model: (a) schematic, (b) side view, and (c) top view.

Fig 4.4(c) illustrates the method to specify the location of a pixel. Take point A marked in Fig. 4.4(c) as an example. First, along the radial direction, the diameter is divided into *2i* parts evenly; then, along the peripheral direction, 2π is divided into *2j* parts evenly. As a result, the whole area is divided by a number of circles. In this thesis, the radius was divided into m parts, and the 2π was divided into m parts as well. Thus, in each layer, m^2 pixels were obtained in total. Let $\mathrm{n} = m^2$, thus *n* denotes the number of pixels in each layer.

4.3.2 Pixel degradation

Consider that the 3D multi-layer model is composed of N pixels. To define the location of a pixel, (i, j, l) is introduced, where i denotes the i^{th} circle in radius direction, j denotes the j^{th} pixel in the circumferential direction (counter-clockwise), and l denotes the l^{th} layer.

There are three statuses of pixels: non-degradable pixels, degraded pixels, and pores. Let $P(i, j, l)$ denote the status of a pixel located at (i, j, l), i.e., non-degraded (1), degraded (0), and pore (-1).

$$P(i,j,l) = \begin{cases} 1 & \text{for non-degraded pixel} \\ 0 & \text{for degraded pixel} \\ -1 & \text{for pores} \end{cases} \tag{4-2}$$

There were several assumptions behind the subsequent model development:

Assumption 1: The pixels are non-degraded at the beginning of a degradation process, and when the degradation process starts, the pixels in the boundary change to the status of pore.

Assumption 2: A degraded pixel becomes a pore only when all its neighboring pixels become pores. A new function $x(i,j,l)$ is thus introduced to capture this assumption.

$$x(i,j,l) = \begin{cases} 1 & P(i,j,l) = 1 \\ 0 & \text{otherwise} \\ -1 & P(i,j,l) = 0 \text{ AND } P(i \pm 1, j \pm 1, l \pm 1) = -1 \end{cases} \quad (4\text{-}3)$$

4.3.3 Degradation Modelling

4.3.3.1 Lifetime of a pixel

In this section, the expected value of the lifetime of a pixel *i* ($t_{\text{lifetime-}i}$) and the lifetime of the whole set of pixels (N pixels) ($t_{\text{lifetime-}N}$) will be discussed first. Then, the random nature of $t_{\text{lifetime-}i}$ and $t_{\text{lifetime-}N}$ will be addressed. It is noted that eventually, the lifetime of the whole set of pixels, which is also called the lifetime of a chitosan scaffold, shall be found.

A pixel is considered degraded once its lifetime expires (Göperich, 1997). The determination of the lifetime of a pixel is based on the assumption that the degradation of a pixel is a random process, particularly following an exponential distribution (Drake, 1988). Let $e(t)$ denote the probability that a pixel degrades at time *t*. The $e(t)$ is then expressed by

$$e(t) = \lambda e^{-\lambda t} \tag{4-4}$$

where *t* denotes the time a pixel is degraded, and λ is degradation rate, which is a constant.

In this thesis, the conjoint thermal and enzymatic effect is considered in such a way that the relative activity (r) of lysozyme is proportional to the degradation rate, i.e.,

$$\lambda = kr \tag{4-5}$$

where k is a constant. Let $\tilde{e}(t)$ denote the probability that a pixel degrades at time *t* in the lysozyme solution at a certain temperature (T). $\tilde{e}(t)$ can be obtained by combining Equation (4-5) and Equation (4-6), i.e.,

$$\tilde{e}(t) = kre^{-krt} \tag{4-6}$$

Substituting Equation (4-1) into Equation (4-6) leads to the probability that a pixel degrades at time *t* in the lysozyme solution at temperature T:

$$\tilde{e}(t) = 1.6e^{0.11T}ke^{-1.6e^{0.11T}kt} \tag{4-7}$$

The expected value of the lifetime of a pixel, $E(t_{\text{lifetime-i}})$, can be found from Equation (4-7), i.e.,

$$E(t_{\text{lifetime-i}}) = \frac{1}{1.6e^{0.11T}k} \tag{4-8}$$

For N pixels, they all follow an exponential kinetics, and the probability distribution of the whole set (i.e., N pixels) can be expressed by

$$\widetilde{e_N}(t) = 1.6e^{0.11T}ke^{-1.6e^{0.11T}kt}(1 + \frac{1}{2} + \cdots + \frac{1}{N}) \tag{4-9}$$

The expected value of the whole set of pixles, $E(t_{\text{lifetime-N}})$ is

$$\mathrm{E}(t_{\text{lifetime}-\mathrm{N}}) = \frac{1}{1.6e^{0.11T}k}(1 + \frac{1}{2} + \cdots + \frac{1}{N}) \tag{4-10}$$

Equation (4-10) can be re-arranged to

$$\mathrm{E}(t_{\text{lifetime}-\mathrm{N}}) = \frac{1}{1.6e^{0.11T}k}\ln N \tag{4-11}$$

Let $t_{\text{degradation}}$ stand for the lifetime of a chitosan scaffold. Noticing $N = nL$, the average degradation time of a chitosan scaffold, $\bar{t}_{\text{degradation}}$, can be found from the following equation, i.e.,

$$\bar{t}_{\text{degradation}} = \text{E}(t_{\text{degradation}}) = \frac{1}{1.6e^{0.11T_k}} \ln(nL) \tag{4-12}$$

According to the probability theory, the cumulative distribution function F(x) of a random variable *x* can be represented by $F(x) = \sigma$, where σ is a random number that is generated by following a Uniform Distribution within the interval of $[0,1]$. Noticing that *x* is lifetime-i and the probability distribution function is an exponential function, i.e., Equation (4-7), the equation to calculate $t_{\text{lifetime}-\text{i}}$ can be found, i.e.,

$$t_{\text{lifetime-i}} = -\frac{1}{1.6e^{0.11T_k}} \ln(1 - \sigma) \tag{4-13}$$

4.3.3.2 Mass loss

After a pixel has degraded, it is not straightforwardly converted to mass loss, as mentioned before when Equation (4-3) was introduced. For the convenience of computation, a preference is given to use "1" to represent the pore status. For this reason, a new function $s(x_{i,j,l})$ is introduced as follows:

$$s(x_{i,j,l}) = \begin{cases} 1, & x(i,j,l) = -1 \\ 0, & \text{otherwise} \end{cases} \quad (4\text{-}14)$$

Mass loss ΔM can now be viewed as the process that a pixel changes its status from the non-degraded status to the pore status. At the beginning, there are N non-degraded pixels. With time going on, pixels change to the pore status. Mass loss can simply be expressed by N minus the number of pores, i.e.,

$$\Delta M = 1 - \frac{1}{\mathrm{n}l}\sum_{l=1}^{l=L}\sum_{j=1}^{j=m}\sum_{i=1}^{i=\mathrm{m}} s(x_{i,j,l}) \quad (4\text{-}15)$$

Note that $N = nL$.

4.3.3.3 Estimation of constant k

In Equation (4-13), constant k should be estimated. This can be done from Experiment II in Chapter 3, in particular the information in Fig. 3.5(c) and Table F.1(b). For the convenience of readers, this information is reproduced here in Table 4.2 below.

Table 4.2. Mass loss information obtained from Experiment-II in Chapter 3

Degradation Time	Temperature	Mass Loss
72h	50°C	90%

This information is then applied by Equation (4-12) to determine k. Note that mass loss is proportional to degradation. The degradation time in Equation (4-12) should be calculated as 72(0.9)=64.8. Substituting $\bar{t}_{\text{degradation}} = 64.8$ and T=50 in Equation (4-12) leads to *k.* The *k* is determined by the total number of pixels (Fig. 4.5).

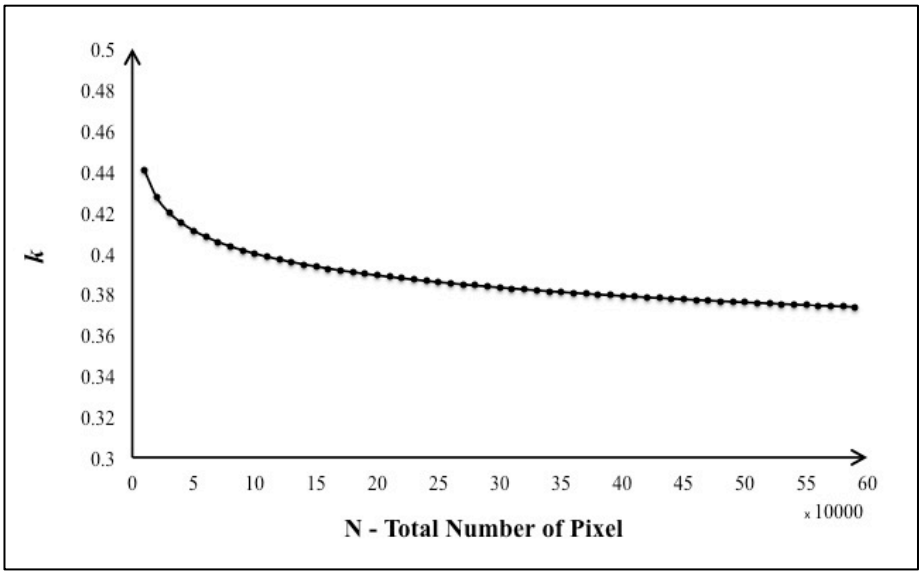

Figure 4.5. The *k* value with different pixle numbers (N).

4.3.3.4 Degradation simulation

A complete degradation model can now be established from the assembly of the developed equations, namely Equation (4-2) for pixel statuses, Equation (4-13) for the prediction of a pixel's lifetime, and Equations (4-3), (4-14), (4-15) for calculating mass loss of a complete scaffold. In the following, a complete simulation procedure is presented.

Step 1: Generate pixels layer by layer. Each pixel then gets a "coordinate" (i, j, l), where $i = 1,2,\cdots,\mathrm{m};\ j = 1,2,\cdots,\mathrm{m};\ l = 1,2,\cdots,\mathrm{L}$.

Step 2: Calculate the lifetime of each pixel using Equation (4-13).

Setp 3: Calculate mass loss using Equation (4-15) while updating the statuses of the pixels using Equation (4-3) and (4-14).

Fig. 4.6 shows the simulation result of mass loss, where the non-degradable pixel is represented by blue points and the pore pixel by white points (or blanks). Particularly, Fig. 4.6(a) is the degradation status at t=0 and Fig. 4.6(b) is the degradation status at t=24 hours.

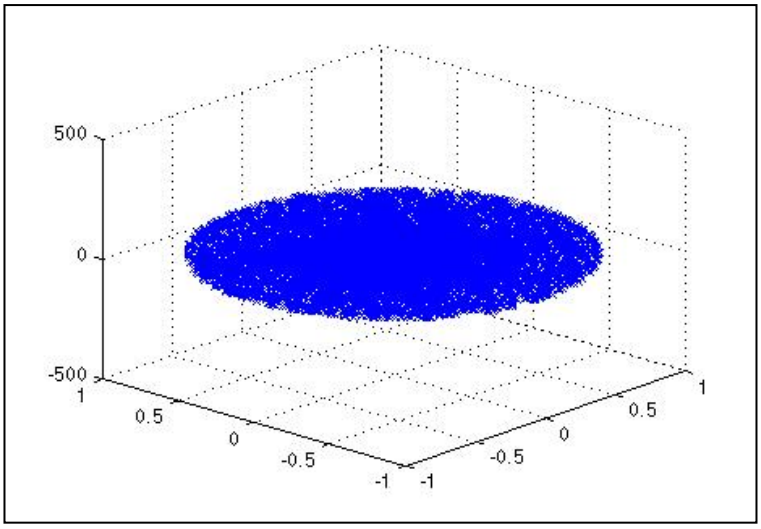

(a)

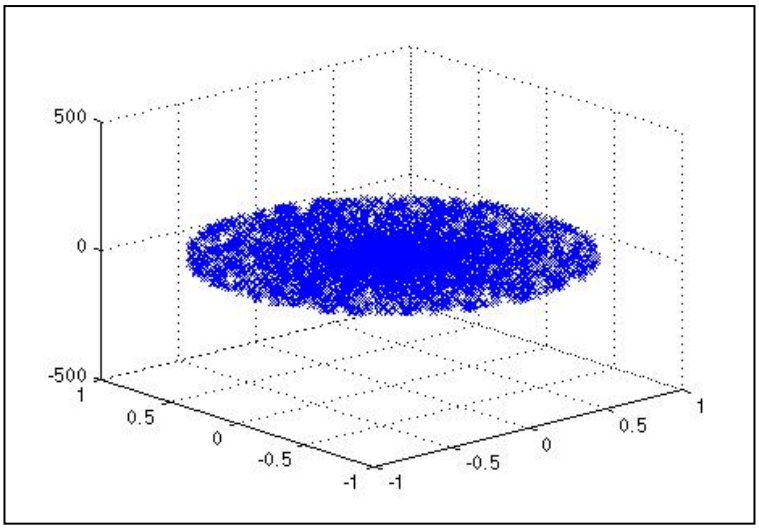

(b)

Figure 4.6. The output of mass loss simulation: (a) initial time and (b) after 24 h.

4.3.3.5 Model validation and sensitivity analysis

Validation of the model is presented in this section. The degradation with respect to time is simulated with different numbers of pixels: (1) N=80,000, L=8, m=100; N=40,000, L=4, m=100; N=20,000, L=2, m=100. Temperature is set to be 37°C. The experiment result is obtained from the experiment described in Section 4.2.2.3. Fig. 4.7 shows a comparision of the simulation and experiment results.

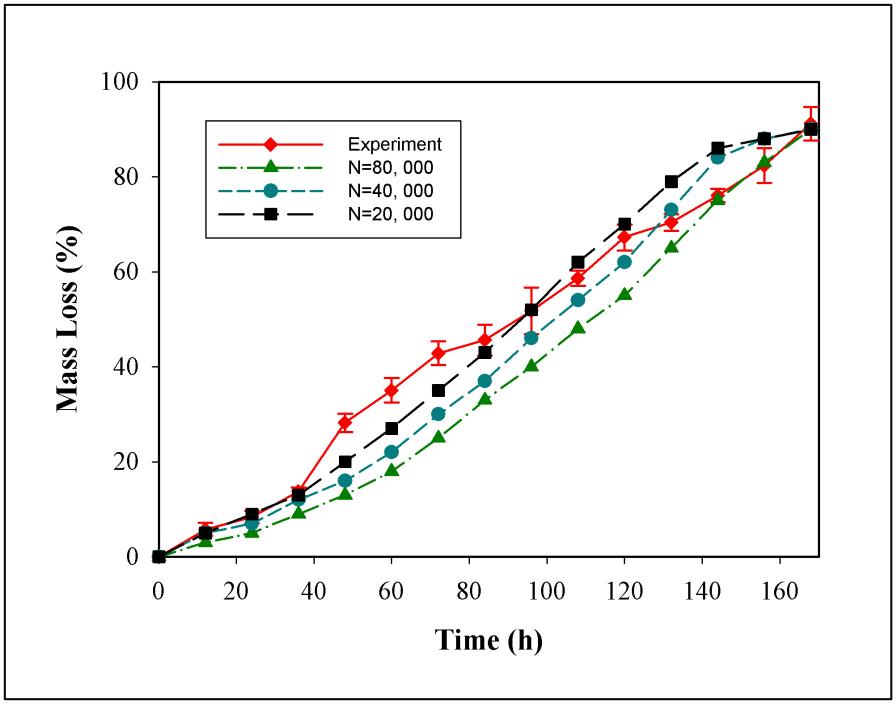

Figure 4.7. Comparison of the simulation result and experiment result of mass loss and degradation time. Model: black (squre), N=20,000, L=2, m=100; (2) blue (circle), N=40,000, L=4, m=100; (3) green (triangle), N=80,000, L=8, m=100.

In Fig. 4.7, all the simulation results show a similar trend as the experiment result, which gives an evidence that the model is valid to predict the degradation of chitosan

scaffold. Another evidence of the validity of the model is that the complete mass loss (i.e., 90% in Fig. 4.7) predicted by the model and that from the experiment are in an excellent agreement. Further, the simulation results with 3 fixed pixel numbers and layer number overlaped with experiment result within a different time interval. The 2-layer model (N=20,000, L=2, m=100) overlaps the experiment result in the first 5 days; while the 8-layer model (N=80,000, L=8, m=100) match the exerpriment well in the last 2 days.

The different performances of three N value, which affect constant *k* (Fig. 4.5), may imply that during degradation process, while mass loss of chitoan film, the *k* might change thereafter. Nevertheless, there are a couple of reasons responsible for the discrepancies between the simulation result and the experiment result. The first reason is that chitosan scaffold is not perfect with some cracks, while the 3D structure model does not capture these characteristics. The second reason is that the geometric shape of the chitosan scaffold used in the experiment was not regular as a cylinder, while the 3D structure model assumes a cylinder.

4.4 Discussions and Conclusion

This chapter presented a comprehensive model for chitosan degradation prediction. A multi-layer structure model for chitosan scaffold was defined first, which is composed of a number of films and a number of pixels on each film. The degradation of the scaffold was then considered as an aggregated degradation from all pixels. A model

for mass loss with consideration of a conjoint thermal and enzymatic effect (lysozyme in this case) was then built. It is noticed that the model developed in this thesis differs from the one develped by Göperich (1997) and Siepmann (2002) in that the model developed in this thesis takes into account the conjoint thermal and enzymatic effect; while their model has only considered enzymatic effect. The model was compared with the experiment, which has shown a promise of the model in predicting mass loss with respect to time (or mass loss dynamics).

CHAPTER 5

REAL-TIME MEASUREMENT OF DEGRDATION RATE

5.1 Introduction

Chapter 4 discussed an improved model of chitosan scaffold degradation. While the model is useful to predict degradation rate, the model cannot be used for degradation control in a feedback manner. To achieve the real-time control of degradation rate, an important step is sensing degradation rate in real-time. In this thesis, degradation is considered as mass loss, so measurement of degradation rate becomes to be measurement of mass loss. On a general note, real-time mass loss measurement is not well studied according to the literature review in Chapter 2. In this chapter, a preliminary study on this topic is described. The general idea was to make a so-called conductive polymer mixture by carbon nanotube (CNT) and to make use of it to build a tissue scaffold.

The remaining part of this chapter is organized as follows: Section 5.2 discusses the fabrication procedure for the conductive polymer mixed up with carbon nanotube (CNT-Chi for short). Section 5.3 presents the testing circuit. Section 5.4 presents results with discussion. Section 5.5 gives a conclusion.

5.2 Procedure to Make the CNT-CHI Sensor

5.2.1 Materials

Multi-wall Carbon Nanotube (MCNT), purchased from Shenzhen Nano-Tech Port Co. Ltd., was chosen for this study owing to its success in making film sensors (Miao, 2010). MCNT was first dried in vacuum at 60°C temperature for 24 h prior to solution preparation. Chitosan and lysozyme were purchased from Sigma with the same source as those used in Chapters 3 and 4.

5.2.2 Fabrication of CNT-Chi

Fabrication of degradation sensors was performed in the following steps.

Step 1: Put and dissolved 2 mg of chitosan in 50 mL 3% acetic acid solution at 37°C under constant stirring. The 5 mg CNTs were dispersed with polymer surfactants in the 5 mL prepared chitosan solution by using a sonicator (Probe sonicator 340) for about 60 minutes; see Fig. 5.1 (Miao, 2010).

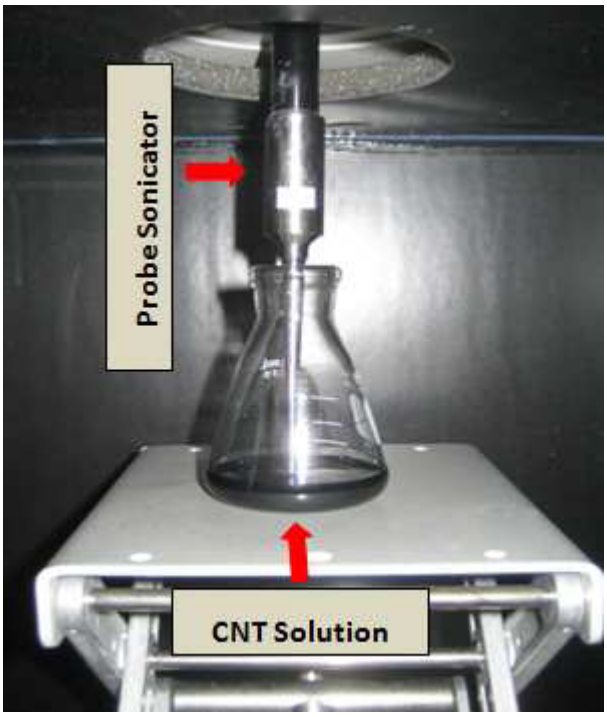

Figure 5.1. CNT-Chi solution (Miao, 2010).

Step 2: Centrifuged the CNT-Polymer solution for 30 minutes by centrifuger (EPPENDORF). The well centrifuged solution was then decanted on the substrate for spin coating by spin coater (Headway Research Inc., US). The spin coating speed can range from 1500 r/min up to 5000 r/min for a few minutes depending on the thickness requirement. After the spin coating, the sample was heated to evaporate the water in an oven at 60ºC (or air dry). The yielded films were cut into square shape; see Fig. 5.2.

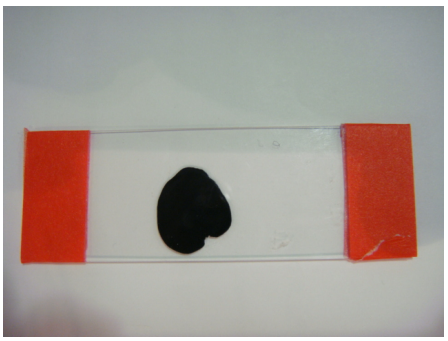

Figure 5.2. CNT-Chi film.

Step 3: Coated gold at the edges of films as a probe by gold coater (Edwards Sputter Coater).

The architecture of such a CNT-Chi film is illustrated in Fig. 5.3.

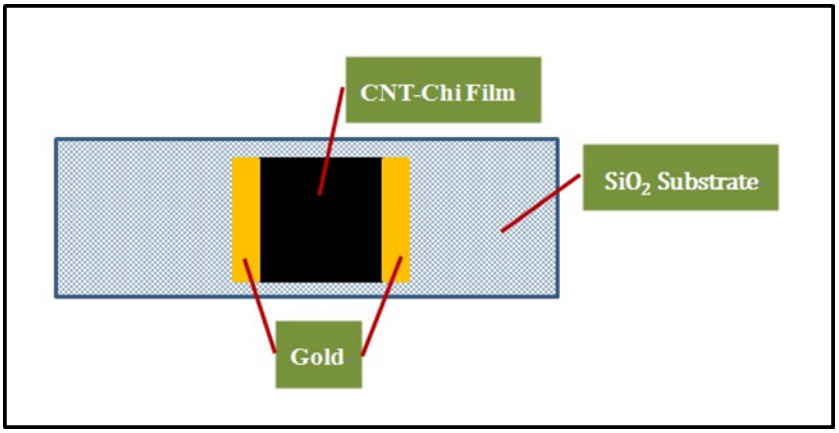

Figure 5.3. CNT-Chi film.

5.3 Measurement of Degradation of the CNT-Chi Film

The electrical resistance of the aforementioned conductive CNT-Chi polymer film was measured to see if it is related to degradation of the CNT-Chi film. A serial circuit was designed for this purpose (see Fig. 5.4). The U_0 denotes the voltage of the whole circuit; R_1 is a fixed resistor with resistance of 9.8 kΩ (to be discussed later); and R_s denotes the resistance of CNT-Chi film.

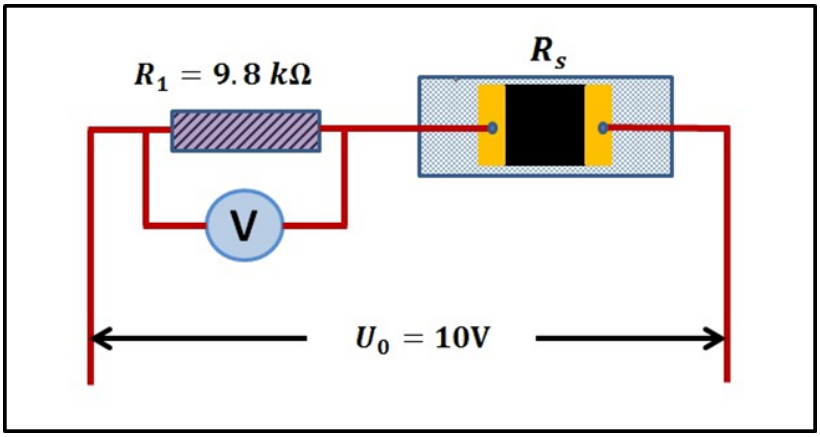

Figure 5.4. Circuit for resistance measurement.

The measurement was processed as follows. First, the circuit was assembled according to Fig. 5.4. Second, power of 10V was added by DC Power Supply to the circuit (Fig. 5.5). Third, the voltage data of R_1 was measured and collected by USB Data Acquisition system (National Instrument Inc.) and displayed in PC by Labview (Fig. 5.6). If the voltage of CNT-Chi film changes, the change of the voltage on R_1 can be observed.

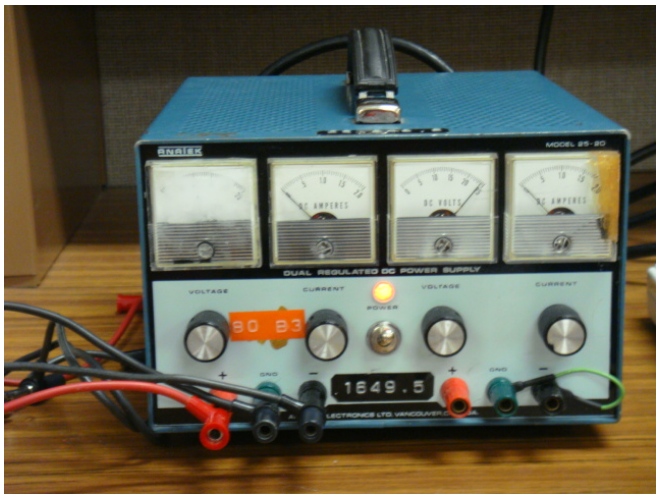

Figure 5.5. DC Power Supply.

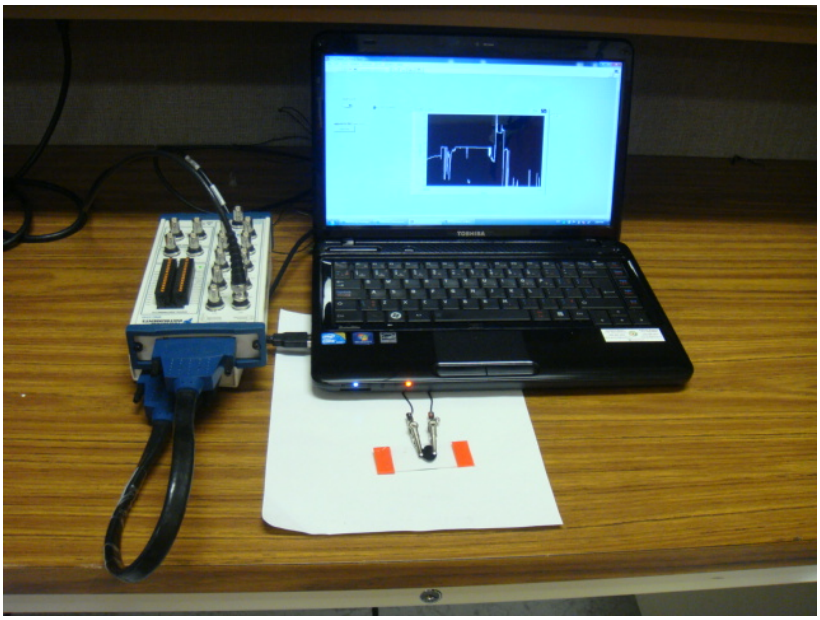

Figure 5.6. USB Data Acquisition System.

5.4 Results and Discussion

Fig. 5.7 shows the voltage on R_1. In the figure, the change in slope is due to the addition of lysozyme onto the CNT-Chi film (in particular by means of drip pipe).

The relationship of voltage and resistance for the system shown in Fig. 5.4 can be represented by the following equation.

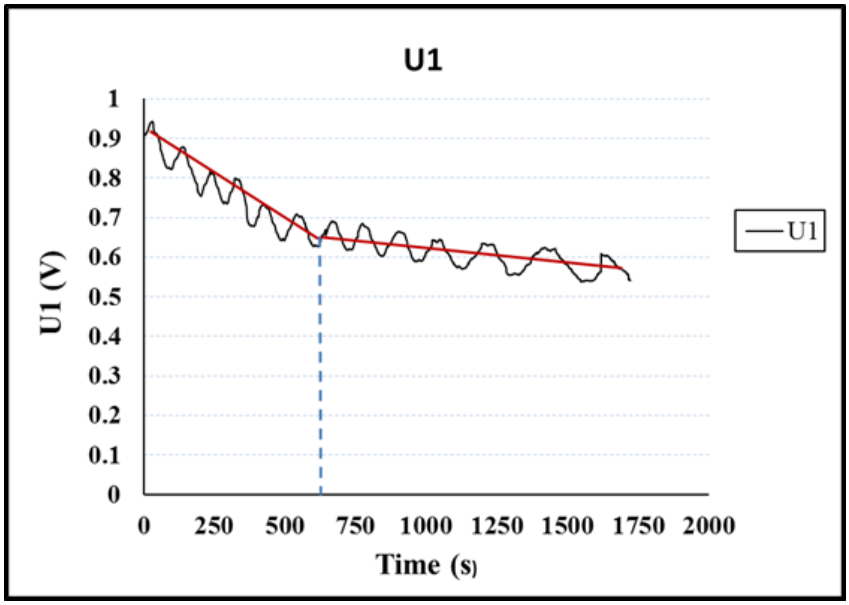

Figure 5.7. Voltage of $\boldsymbol{R_1}$.

$$\begin{cases} U_0 = U_1 + U_S \\ I_0 = I_1 = I_S \\ R_0 = R_1 = R_S \end{cases} \tag{5-1}$$

From Equation (5-1), one can obtain the change in voltage of R_s (see Fig. 5.8).

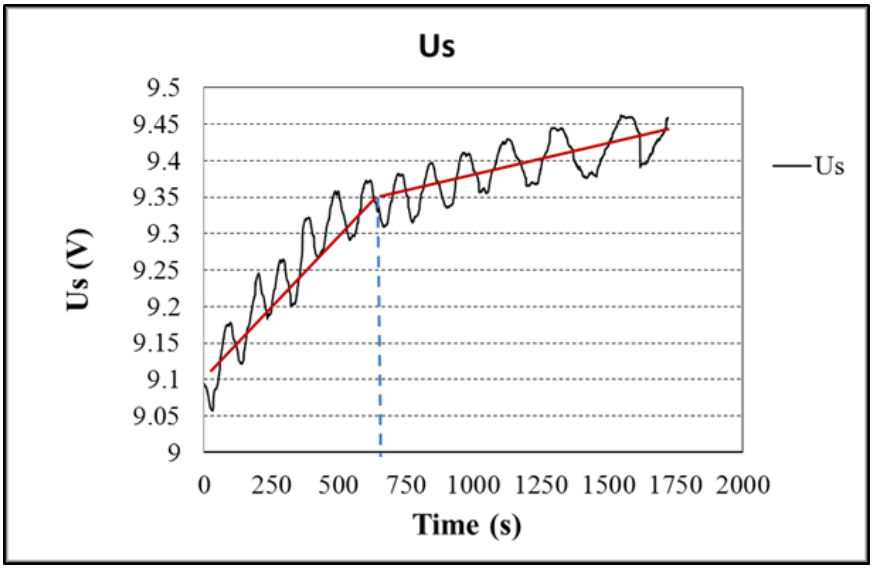

Figure 5.8. Voltage of R_s.

Further, one can get the following equations from the circuit of Fig. 5.4, i.e.,

$$R_1 + R_s = \frac{U_0}{I} \tag{5-2}$$

$$\begin{cases} I = \frac{U_0}{R_0} \\ I_1 = \frac{U_1}{R_1} \\ I_S = \frac{U_S}{R_S} \end{cases} \tag{5-3}$$

$$\frac{U_1}{R_1} = \frac{U_S}{R_S} \tag{5-4}$$

$$R_S = R_1 \frac{U_0 - U_1}{U_1} \tag{5-5}$$

From the above equations, one can get the relationship between R_s and time (Fig. 5.9).

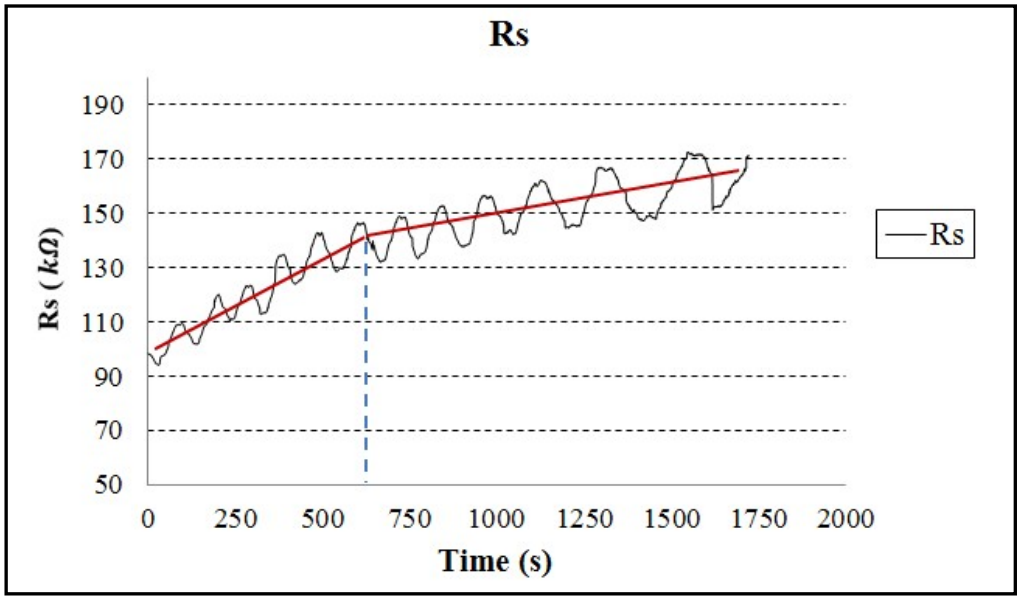

Figure 5.9. Resistance of R_s.

From Fig. 5.7, one can see there is a change in slope at *t*=600 s. This is due to the dilution of lysozyme solution at *t*=600 s. As the concentration of lysozyme solution can affect degradation rate, the result as shown in Fig. 5.9 therefore suggests that the CNT-Chi film is sensitive to degradation rate. The relationship between the resistance and mass loss is plotted in Fig. 5.10. The data analysis shows that the relationship is linear with $R^2 = 0.98$. This result indicates that the CNT-Chi film is promising as a sensor for mass loss measurement.

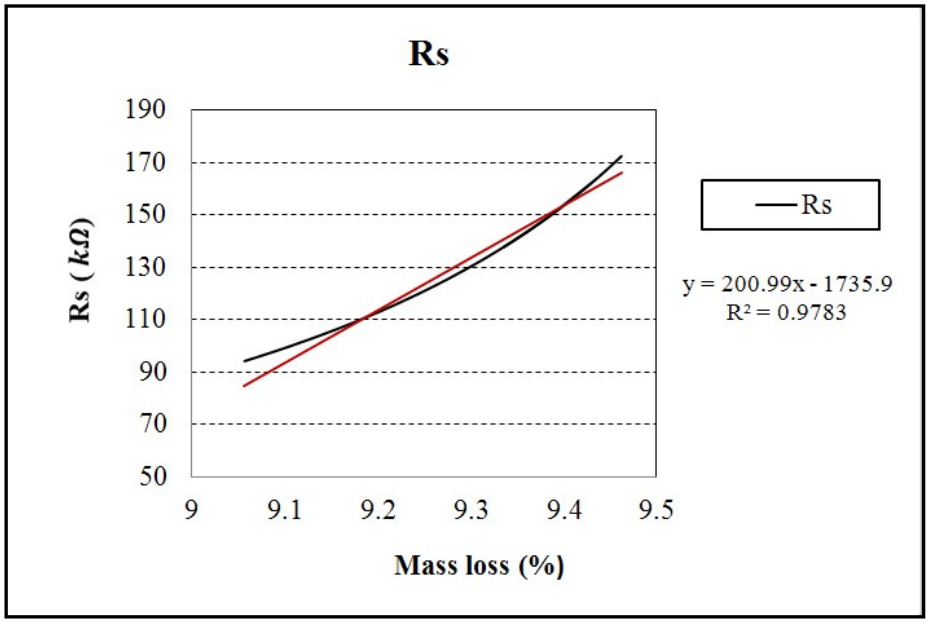

Figure 5.10. Resistance versus mass loss.

5.5 Conclusion

This chapter described a preliminary yet pilot study on sensing mass loss of chitosan films mixed up with CNT (such a film is thus called CNT-Chi film). The following conclusions can be drawn from the study: (1) The change in resistance of the CNT-Chi film has a linear relationship with mass loss; (2) It is promising to build a degradation sensor-scaffold made of the CNT-Chi film. It is noted that such a sensor-scaffold may possibly be built with other biomaterials.

CHAPTER 6

CONCLUSIONS AND RECOMMENDATION

6.1 Overview and Conclusion

This thesis studied the conjoint thermal and enzymatic effect on degradation of chitosan films, modeling of degradation in terms of mass loss, and sensor for real-time measurement of degradation rate. The motivation of the study was to develop a more effective degradation control method for scaffolds which are made of biomaterials, which is in particular called active control of degradation. There were three specific objectives in this study, namely (1) understanding of thermal and enzymatic effects on degradation of chitosan films, (2) modeling of degradation rate of chitosan films in terms of mass loss, and (3) development of a real time sensor for measuring mass loss.

After a comprehensive literature review in Chapter 2, which confirms the necessity of the proposed study, Chapter 3 described the research towards understanding of the conjoint thermal effect and enzymatic effect. The temperature range from 30°C to 50°C was set to examine the thermal effect. Lysozyme was used for studying the enzymatic effect. A statistic experiment was designed, which takes temperature, enzyme, time as independent variable or factor, and mass loss as a dependent variable or response. In general, the experimental study confirmed a significant joint effect of temperature and enzyme.

Following the general philosophy of active control of degradation of tissue scaffolds, Chapter 4 presented the study of modeling of scaffolds made of chitosan by temperature and enzyme as two variables along with time. Again, mass loss was taken as a dependent variable. The study included the following steps. First, a 3D layer by layer model for chitosan films was formulated, which was further viewed as consisting of pixels. Second, an experiment was designed and carried out to obtain the enzymatic function activity with respect to temperature. This activity was a basis for degradation. Third, degradation on one pixel and then that on all pixels in the chitosan scaffold were described based on a stochastic process. The model was validated to show its promise to predict chitosan degradation rate.

Chapter 5 presented the study of biosensors for real-time measurement of mass loss of a tissue scaffold. The general idea that emerged from the study was to use a conductive polymer to build scaffolds. As a result, it may be possible that while such a scaffold is degrading, mass loss is sensed by the effect of conductive polymer. This idea can be made an analogy to human body within which a kind of "strain" sensor goes throughout the whole body. That is to say, the whole human body is sensible to strain. Based on this idea, the following steps were made toward real-time measurement of mass loss of a tissue scaffold. First, a concept called CNT-Chi conductive polymer was adapted to the situation of the present study; in particular chitosan was taken as a matrix over which CNTs were dispersed. The CNT-Chi film

was fabricated. Second, an experiment was carried out to investigate the feasibility of such a CNT-Chi film sensor for the purpose of the current study.

In short, all the three objectives have been achieved. The study has led to the following conclusions:

(1) There is little effect of temperature in the range of 30°C to 50°C on chitosan degradation. In other words, the particular thermal effect alone is not useful to active control of degradation of chitosan.

(2) There is a significant effect of temperature in the range of 30°C to 50°C for the chitosan treated by lysozyme. This particular effect is practical and open to many possible external interventions to adjust temperature *in-situ* in the context of tissue regeneration.

(3) The dynamic model for the chitosan film or scaffold with the Monte Carlo simulation technique appears to be valid to predict degradation rate of chitosan scaffold in terms of mass loss.

(4) The chitosan CNT-Chi film is an excellent sensor for measuring degradation rate of chitosan scaffolds.

(5) The idea of the chitosan CNT-Chi film sensor is promising in further developing a tissue scaffold which has a capability of self-awareness of mass loss. Note that such a scaffold may be called the mass loss sensible (MLS) scaffold.

6.2 Contributions

The study described in this thesis has made the following contributions to the field of tissue scaffold technology and biomaterial devices:

(1) The development of the concept of active control of degradation rate of chitosan film in the application of tissue scaffold - in particular the concept of MLS scaffold.

(2) The finding that to chitosan film, a particular thermal effect (i.e., temperature range of 30°C to 50°C), makes sense to chitosan treated by lysozyme but does not make sense with the particular temperature range alone.

(3) The model that can predict degradation rate for chitosan scaffolds treated by lysozyme with temperature and time as two independent variables.

(4) The chitosan CNT-Chi film sensor for real-time measurement of mass loss.

6.3 Limitations and Future Work

Research described in this thesis is preliminary and has some limitation. Analysis of limitations will be provided in the following. This analysis provides motivation for future work that will be given as well.

The first limitation is that the present study has not considered the effect of concentration of lysozyme. It is likely that the concentration can be a significant

factor. The second limitation is that the modeling process is relatively restrictive to chitosan scaffolds. The third limitation is that the CNT-Chi sensor has only been shown to have a linear relationship in one dimension; however, tissue scaffold degradation happens in a 3D situation.

Several future studies can be suggested. First, the experimental study with consideration of concentration of lysozyme is recommended for future study. Second, in modeling of degradation rate of chitosan, the following aspects need more attention: (1) extension of the structural model to be closer to the real structure of a scaffold; and (2) considering more realistic situations of neighbor pixels in determining whether a degraded pixel should be a pore. Third, the chitosan film sensor needs more tests to see if there is a linear relationship in a 3D situation.

Last, to fully implement the concept of active control of degradation rate of tissue scaffolds, there is a need of several further works: (a) study how to deliver energy to the tissue scaffold to change its temperature and how to deliver enzyme to the tissue scaffold; and (b) study how to transmit signals of mass loss of a tissue scaffold from the tissue scaffold to outside.

LIST OF REFERENCES

Albertsson, A., Qu, X., & Wirse, A. (2000). Effect of lactic / glycolic acid side chains on the thermal degradation kinetics of chitosan derivatives. *Polymer*, *41*, 4841-4847.

Anantram, M. P. & Léonard, F. (2006). Physics of carbon nanotube electronic devices. *Reports on Progress in Physics*, 69(3), 507-561.

Avraham, K. B., Hasson, T., Steel, K. P., Kingsley, D. M., Russell, L. B., Mooseker, M. S., Copeland, N. G., & Jenkins, N. A. (1994). The mouse Snell's waltzer deafness gene encodes an unconventional myosin required for structural integrity of inner ear hair cells. *Nature Genetics, 11*, 369-375.

Balasubramanian, K., & Burghard, M. (2006). Biosensors based on carbon nanotubes. *Analytical and Bioanalytical Chemistry*, *385*(3), 452-468.

Batycky, R. P., Hanes, J., Langer, R, & Edwards, D. A. (1997). A theoretical model of erosion and macromolecular drug release from biodegrading microspheres. *Journal of pharmaceutical sciences*, *86*(12), 1464-77.

Bianco, P., & Robey, P. G. (2001). Stem cells in tissue engineering. *Nature, 414*(6859), 118-121.

Burkersroda, F.V., & Göpferich, A. (1999). An approach to classify degradable polymers, in: Neenean, T., Marcolongo, M., & Valentini, R.F. (Eds.), Symp Press.

Burkersroda, F. V., Schedl, L., & Göpferich, A. (2002). Why degradable polymers undergo surface erosion or bulk erosion. *Biomaterials*, *23*(21), 4221-31.

Carrier, R. L., Papadaki, M., Rupnick, M., Schoen, F. J., Bursac, N., Langer, R., Freed, L. E., & Vunjak-Novakovic, G. (1999). Cardiac tissue engineering: cell seeding,

cultivation parameters, and tissue construct characterization. *Biotechnology and Bioengineering, 64*(5), 580-590.

Chen, Y. L., Lee, H. P., Chan, H. Y., Sung, L. Y., Chen, H. C., & Hu, Y. C. (2007). Composite chondroitin-6-sulfate/dermatan sulfate/chitosan scaffolds for cartilage tissue engineering. *Biomaterials*, *28*(14), 2294-305.

Chen, Y., Zhou, S., & Li, Q. (2011). Acta Biomaterialia Mathematical modeling of degradation for bulk-erosive polymers: Applications in tissue engineering scaffolds and drug delivery systems. *Acta Biomaterialia*, *7*(3), 1140-1149.

Crompton, K. E., Goud, J. D., Bellamkonda, R. V., Gengenbach, T. R., Finkelstein, D. I., & Horne, M. K. (2007). Polylysine-functionalised thermoresponsive chitosan hydrogel for neural tissue engineering. *Biomaterials*, *28*(3), 441-9.

Cunha-Reis, C., Tuzlakoglu, K., Baas, E., Yang, Y., & Haj, A.E. (2007). Influence of porosity and fibre diameter on the degradation of chitosan fibre-mesh scaffold and cell adhesion. *Journal of Materials Science, 18*(2), 195-200.

Dou, H., Yang, W., Tao, K., Li, W., & Sun, K. (2010). Thermal sensitive microgels with stable and reversible photoluminescence based on covalently bonded quantum dots. *Langmuir: the ACS journal of surfaces and colloids*, *26*(7), 5022-5027.

Doyle, J., Francis, B., & Tannenbaum, A. (Ed.). (1990), *Feedback control theory*, New York: Macmillan Publishing Co.

Doyle, J.C. & Stein, G. (1981). Multivariable feedback design: concepts for a classical modern synthesis, *IEEE Trans. Auto. Contorl, 26*, 4-16.

Drury, J. (2003). Hydrogels for tissue engineering: scaffold design variables and applications. *Biomaterials*, *24*(24), 4337-4351.

Fermentation, J. O. F. (1997). Enzymatic Hydrolysis Reaction of Water-Soluble Derivatives with Egg White Lysozyme. *Journal of Fermentation and Bioengineering*, *84*(5), 478-479.

Francis, S. J. K., & Matthew, H. W. T. (2000). Application of chitosan-based polysaccharide biomaterials in cartilage tissue engineering: a review. *Biomaterials, 21*, 2589.

Franklin, G. F., Powell, J. D., & Emami-Naeini, A. (2010). Feedback control of dynamic systems (6^{th} edition), Prentice-Hall.

Freier, T., Koh, H. S., Kazazian, K., & Shoichet, M. S. (2005). Controlling cell adhesion and degradation of chitosan films by N-acetylation. *Biomaterials, 26,* 5872-5878.

Gerecht, S., Townsend, S. A., Pressler, H., Zhu, H., Nijst, C. L. E., & Bruggeman, J. P. (2007). A porous photocurable elastomer for cell encapsulation and culture. *Biomaterials*, *28*(32), 4826-35.

Göpferich, A. (1996). Mechanisms of polymer degradation and erosion. *Biomaterials*, *17*(2), 103-14.

Göpferich, A. (1997). Bioerodible implants with programmable drug release. *Journal of Controlled Release. 44*, 271-281.

Göpferich, A. (1997). Polymer Bulk Erosion. *Society*, *9297*(96), 2598-2604.

Green, J. J., Zugates, G. T., Tedford, N. C., Huang, Y. H., Griffith, L. G., & Lauffenburger, D. (2007). Combinatorial Modification of Degradable Polymers Enables Transfection of Human Cells Comparable to Adenovirus. *Advanced Materials*, *19*(19), 2836-2842.

Guimard, N., Gomez, N., & Schmidt, C. (2007). Conducting polymers in biomedical engineering. *Progress in Polymer Science*, *32*(9), 876-921.

Hauft, S. M., Kim, S. H., Schmidt, G. H., Pease, S., Rees, S., Harris, S., Roth, K. A., Hansbrough, R. H., Cohn, S. M., Ahnen, D. J., Wright, N. A., Goodlad, R. A., & Gordon, J. I. (1992). Expression of SV-40 T antigen in the small intestinal epithelium of transgenic mice results in proliferative changes in the crypt and reentry of Villus-Associated enterocytes into the cell cycle but has no apparent

effect on cellular differentiation programs and does not cause neoplastic rransformation. *The Journal of Cell Bioloty, 117*(4), 825-839.

Hirano, Y., & Mooney, D. J. (2004). Peptide and Protein Presenting Materials for Tissue Engineering. *Advanced Materials*, *16*(1), 17-25.

Höpfenberg, H. B., & Hsu, K. C. (2004). Swelling-controlled, constand rate delivery systems. *Polymer Engineering and Science, 18*(15), 1186-1191.

Hu, P., Zhang, J., Li, L., Wang, Z., & Estrela, P. (2010). Carbon Nanostructure-Based Field-Effect Transistors for Label-Free Chemical/Biological Sensors. *Sensors (Peterborough, NH)*, 10(5), 5133-5159.

Huebsch, N., & Mooney, D. J. (2009). Inspiration and application in the evolution of biomaterials. *Nature*, *462*(7272), 426-32.

Hutmacher, D. W. (2001). Scaffold design and fabrication technologies for engineering tissues – state of the art and future perspectives. *J. Biomater. Sci. Polymer Edn, 12*(1), 107-124.

Illum, L. (1998). Chitosan and its use as a pharmaceutical excipient. *Pharmaceutical Research, 15*(9), 1326-1332.

Imoto, T., Ueda, T., & Tamura, T. (1994). Lysozyme requires fluctuation of the active site for the manifestation of activity. *Protein Engineering*, *7*(6), 2-5.

Isidori, A., Schuppen, J. H., Sontag, E. D., Thoma, M., & Krstic, M. (1999). Communications and control engineering, New York, Springer.

Khademhosseini, A., & Langer, R. (2007). Microengineered hydrogels for tissue engineering. *Biomaterials*, *28*(34), 5087-92.

Khademhosseini, A., Vacanti, J. P., & Langer, R. (2009). Progress in tissue engineering. *Scientific American*, *300*(5), 64-71.

Kim, K. (2003). Control of degradation rate and hydrophilicity in electrospun non-woven poly(L-lactide) nanofiber scaffolds for biomedical applications. *Biomaterials*, *24*(27), 4977-4985.

Kim, Y. S., & Pivovar, B. S. (2010). Moving Beyond Mass-Based Parameters for Conductivity Analysis of Sulfonated Polymers. *Annual Review of Chemical and Biomolecular Engineering*, *1*(1), 123-148.

Kumar, D. P., Dutta, J., & Tripathi, V. S. (2004). Chitin and chitosan: Chemistry, properties and applications. *Journal of Sciencetific & Industrial Research, 63*, 20-31.

Kumar, M. N. V. R., Muzzarelli, R. A. A., Muzzarelli, C., Sashiwa, H., & Domb, A. J. (2004). Chitosan chemistry and pharmaceutical perspectives. *Chemical reviews*, 104(12), 6017-6084.

Langer, R. (2000). Biomaterials in Drug Delivery and Tissue Engineering: One Laboratory's Experience. *Accounts of Chemical Research*, 33(2), 94-101.

Langer, R. (2007). Tissue Engineering: Perspectives, Challenges, and Future Directions. *Tissue Engineering,* 13(1), 1-2.

Langer, R., & Peppas, N. (1983). Chemical and physical structure of polymers as carriers for controlled release of bioactive agents: a review, *J. Macromol. Sci.,* 23: 61-126, 1983.

Langer, R., & Vacanti, J. P. (1993). Tissue Engineering. *Science*, 12(1), 347-359.

Lee, J. (2003). Thermal and mechanical characteristics of poly(?-lactic acid) nanocomposite scaffold. *Biomaterials*, 24(16), 2773-2778.

Lee, K. Y., & Mooney, D. J. (2001). Hydrogels for Tissue Engineering. *Surgery*, *101*(7), 1869-1880.

Lendlein, A., & Langer, R. (2002). Biodegradable, Elastic Shape-Memory Polymers for Potential Biomedical Applications. *Science,* 296(5573), 1673-1676.)

Levine, S. E., Fox, J. M., Blanch, H. W., & Clark, D. S. (2010). A RTICLE A Mechanistic Model of the Enzymatic Hydrolysis of Cellulose. *Biotechnology*, *107*(1), 37-51.

Li, X., Petersen, L., Broderick, S., Narasimhan, B., & Rajan, K. (2011). Identifying factors controlling protein release from combinatorial biomaterial libraries via hybrid data mining methods. *ACS Combinatorial Science*, 13(1), 50-58.

Li, C., & Chou, T. W. (2004). Mass detection using carbon nanotube-based nanomechanical resonators. *Applied Physics Letters*, 84(25), 5246.

Lyu, S., Schley, J., Loy, B., Lind, D., Hobot, C., Sparer, R.. (2007). Kinetics and time-temperature equivalence of polymer degradation. *Biomacromolecules*, 8(7), 2301-10.

Madihaly, S. V., & Matthew, H. W. (1999). Porous chitosan scaffolds for tissue engineering. *Biomaterias.* 20(12), 1133-42.

Maeda, R., Matsumoto, M., & Kondo, K. (1997). Enzymatic hydrolysis reaction of water-soluble chitin derivatives with egg white lysozyme. *Journal of Fermentation and Bioengineering,* 84(5), 478-479.

Mahdavi, A., Ferreira, L., Sundback, C., Nichol, J. W., Chan, E. P., & Carter, D. J. D. (2008). A biodegradable and biocompatible gecko-inspired tissue adhesive. *Proceedings of the National Academy of Sciences of the United States of America*, 105(7), 2307-12.

Miao, Y. (2010). A New Strain Sensor Based on Pure CNT Films. Available online: http://library2.usask.ca/theses/available/etd-08172010-165151/.

Neeley, W. L., Redenti, S., Klassen, H., Tao, S., Desai, T., & Young, M. J. (2008). A micro-fabricated scaffold for retinal progenitor cell grafting. *Biomaterials*, 29(4), 418-26.

Nordtveit, R. J., Vhrum, K. M., & Smidsrød, O. (1994). Degradation of fully water-soluble, partially N-acetylated chitosans with lysozyme. *Biomaterials*, 23, 253-260.

Park, S., Lee, K. B., Choi, I. S., Langer, R., & Jon, S. (2007). Dual functional, polymeric self-assembled monolayers as a facile platform for construction of patterns of biomolecules. *Langmuir: the ACS journal of surfaces and colloids*, *23*(22), 10902-5.

Park, T. H. & Shuler, M. L. (2003). Integration of cell culture and microfabrication technology. *Biotechnology progress*, 19(2), 243-53.

Pawlak, A. & Mucha, M. (2002). Thermogravimetric and FTIR studies of chitosan blends. *Thermochimica Acta,* 396, 153-166.

Petersen, L. K., Sackett, C. K., & Narasimhan, B. (2010). Novel, High Throughput Method to Study in-vitro Protein Release from Polymer Nanospheres. *Journal of Combinatorial Chemistry, 12*(1), 51-56.

Prichard, H. L., Reichert, W. M., & Klitzman, B. (2007). Adult adipose-derived stem cell attachment to biomaterials. *Biomaterials*, *28*(6), 936-46.

Ratner, B. D., Hoffman, A. S., Schoen, F. J., & Lemons, J. E. (Ed.). (2003). Biomaterials Science: An Introduction to Materials in Medicine. *San Diego*: Academic Press

Kumar, M. N. V. R. (2000). A review of applications of chitin and chitosan. *Reactive and Functional Polymers*, *46*(1), 1-27.

Rivest, C., Morrison, D. W. G., Ni, B., Rubin, J., Yadav, V., & Mahdavi, A. (2007). Microscale hydrogels: fabrication, applications and mechanical properties. *Mechanics of Materials and Structures*, *2*, 756-794.

Rothstein, S. N., Federspiel, J., & Little, S. R. (2008). A simple model framework for the prediction of controlled release from bulk eroding polymer matrices. *Biomaterials*, *18*, 1873-1880.

Sackett, C. K. & Narasimhan, B. (2011). Mathematical modeling of polymer erosion: Consequences for drug delivery. *International Journal of Pharmaceutics*, *418*(1), 104-114.

Salton, M. R. J. (1952). Cell wall of *micrococcus lysodeikticus* as the substrate of lysozyme. *Nature, 4331*, 746-748.

Sheridan, M. H., Shea, L. D., Peters, M. C., & Mooney, D. J. (2000). Bioabsorbable polymer scaffolds for tissue engineering capable of sustained growth factor delivery. *Journal of controlled release: official journal of the Controlled Release Society*, *64*(1-3), 91-102.

Siepmann, J. & Göpferich, A. (2001). Mathematical modeling of bioerodible , polymeric drug delivery systems. *Advanced Drug Delivery Reviews*, *48(4),* 229-247.

Siepmann, J., Faisant, N., & Benoit, J. (2002). A new mathematical model of drug release from bioerodible microparticles using Monte Carlo Simulations. *Pharmaceutical Research*, *19*(12), 1885-1893.

Sikorski, P., Stokke, B. T., Sørbotten, A., Vårum, K. M., Horn, S. J., & Eijsink, V. G. H. (2005). Development and Application of a Model for Chitosan Hydrolysis by a Family 18. *Online*, *77*, 273-285.

Smart, S. K., Cassady, A. I., Lu, G. Q., & Martin, D. J. (2006). The biocompatibility of carbon nanotubes. *Scanning*, *44*, 1034-1047.

Soares, J. S. & Zunino, P. (2010). A mixture model for water uptake, degradation, erosion and drug release from polydisperse polymeric networks. *Biomaterials*, *31*(11), 3032-42.

Stock, U. A. & Vacanti, J. P. (2001). Tissue Engineering: current and prospects. *Annu Rev Med., 52*, 443-51.

Suárez, N., Brocchini, S., & Kohn, J. (1998). The study of water uptake in degradable polymers by thermally stimulated depolarization currents. *Biomaterials*, *19*(24), 2347-56.

Tachaboonyakiat, W. & Serizawa, T. (2002). Inorganic – organic polymer hybrid scaffold for tissue engineering - II: Partial enzymatic degradation of hydroxyapatite – chitosan hybrid. *Polymer*, *13*(9), 1021- 1032.

Thompson, C. B. (1995). Apoptosis in the pathogenesis and treatment of disease. *Science, 267*(5203), 1456-1462.

Thompson, P. A., Lade, S., Webster, H., Ryan. G., & Prince, H. M. (2010). Effusion-associated anaplastic large cell lymphoma of the breast: time for it to be defined as a distinct clinico-pathological entity37. Haematologica., 95(11), 1977-9.

Tomihata, K. & Ikada. Y. (1997). In-vitro and *in-vivo* degradation of films of chitin and its deacetylated derivatives. *Biomaterials, 18*, 567-575

Tsaih, M. L. & Chen, R. H. (2003). Effect of degree of deacetylation of chitosan on the kinetics of ultrasonic degreeion of chitosan. Journal of Applied Polyer, *90*(13), 3526-3531.

Vacanti, J. P., Morse, M. A., Saltzman, W. M., Domb, A. J., Perez-Atayde, A., & Langer, R. (2006). Selective cell transplantation using bioabsorbable artificial polymers as matrices. *Journal of Pediatric Surgery,. 23*(1), 3-9.

Vårum, K. M., Myhr, M. M., Hjerde, R. J. N., & Smidsrod, O. (1997). *In-vitro* degradation rates of partially N-acetylated chitosans in human serum. *Carbohydrate Research, 299*, 99-101.

Vaidya, R., Tender, L. M., Bradley, G., Brien, M. J., Cone, M., & López, G. P. (1998). Computer-controlled laser ablation: a convenient and versatile tool for micropatterning biofunctional synthetic surfaces for applications in biosensing and tissue engineering. *Biotechnology progress*, *14*(3), 371-377.

Vocadlo, D. J., Davies, G. J., Laine, R., & Withers, S. G. (2001). Catalysis by hen egg-white lysozyme proceeds via a covalent intermediate. *Nature, 412*(6849), 835-838.

Weiner, A. A., Shuck, D. M., Bush, J. R., & Prasad, S. V. (2007). *In-vitro* degradation characteristics of photocrosslinked anhydride systems for bone augmentation applications. *Biomaterials*, *28*(35), 5259-70.

Wilson, A. D., & Baietto, M. (2011) Advances in electronic-nose technologies development for biomedical applications. *Sensor, 11*, 1105-1176.

Wilson, A. R. & Muscat, R. F. (2010). Novel thin wire paint and sealant degradation sensor. *Sensors & Actuators: A. Physical*, *169*(2), 301-307.

Wilson, G.S. & Gifford, R. (2005) Biosensors for real-time *in-vivo* measurements. *Biosensors and Bioelectronics, 20*, 2388-2403.

Wood, K. C., Azarin, S. M., Arap, W., Pasqualini, R., Langer, R., & Hammond, P. T. (2008). Tumor-targeted gene delivery using molecularly engineered hybrid polymers functionalized with a tumor-homing peptide. *Bioconjugate chemistry*, *19*(2), 403-5.

Yang, F., Mei, Y., Langer, R., & Anderson, D. G. (2009). High throughput optimization of stem cell microenvironments. *Combinatorial chemistry & high throughput screening*, *12*(6), 554-61.

Yoshimura, K., Toibana, A., & Nakahama, K. (1988). "Human lysozyme: sequencing of a cDNA, and expression and secretion by Saccharomyces cerevisiae". *Biochem. Biophys. Res. Commun. 150*(2), 794–801.

Yu, R., Chen, H., Chen, T., & Zhou, X. (2007). Modeling the Drug Release From 3D Multi-layer Microstructure with Micro-chambers. *Polymer*, 5037(5116), 558-561.

Zheng, J. P., Wang, C. Z., Wang, X. X., & Wang, H. Y. (2007). Preparation of biomimetic three-dimensional gelatin / montmorillonite – chitosan scaVold for tissue engineering. *In-vitro*, *67*, 780-788.

Zhou, Q., Lau, S., Wu, D., & Shung, K. K. (2011). Progress in Materials Science Piezoelectric films for high frequency ultrasonic transducers in biomedical applications. *Progress in Materials Science*, *56*(2), 139-174.

Zygourakis, K. & Markenscoff, P. A. (1996). Computer-aided design of bioerodible devices with optimal release characteristics: a cellular automata approach. *Biomaterials,* 17, 125–13.

APPENDIX A

CONTROL THEORY FOR SCAFFOLD DEGRADATION CONTROL

This thesis proposed a new paradigm of scaffold degradation control, that is, closed-loop and real-time control. Extraordinary developments have been taken place since 1980 in feedback control theory (Doyle *et al.,* 1990). A control system has three components: a plant, which is the object to be controlled; a sensor, which is used to measure the output of the plant; and a controller, which is to regulate the plant's input (Franklin *et al.*, 2010). The block diagram of a control system is shown in Fig. A.1. In scaffold degradation control problem, the scaffold is considered as a plant; degradation sensor is the sensor; and a specific degradation model of the scaffold is a part of the controller which generates a scheme of energy that is input to the plant.

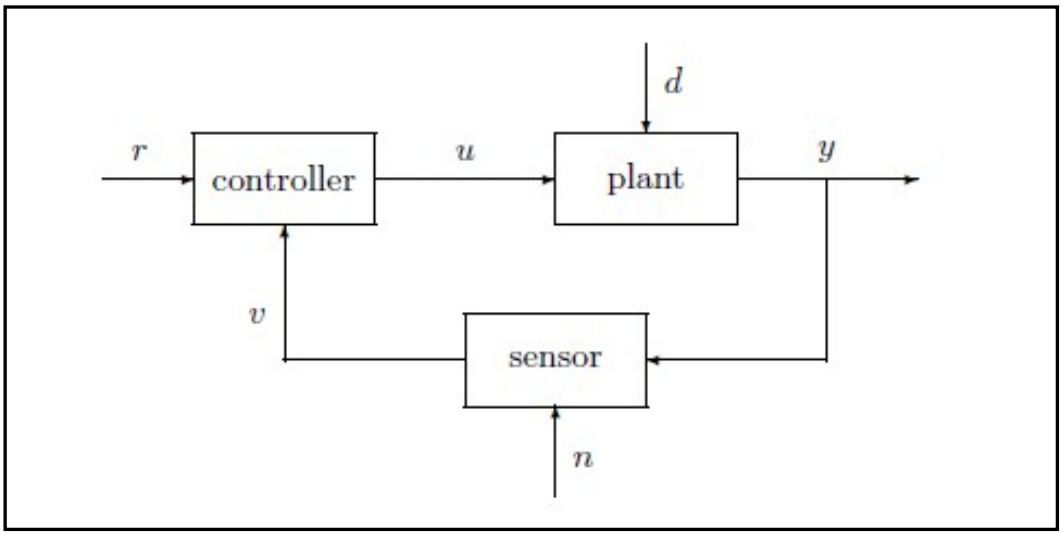

Figure A.1. Control system (Doyle et al., 1990).

Table A.1. List of interpretations for signals in Fig. A.1

Signals	Interpretations
r	reference or command input
v	sensor output
u	actuating signal, plant input
d	external disturbance
y	plant output and measured signal
n	sensor noise

According to Isidori *et al.* (1999), the scenario of designing a control system generally involves 11 steps: (1) study the system to be controlled and decide what types of sensors and actuators will be used; (2) model the resulting system to be controlled; (3) simplify the model if necessary to that it is tractable; (4) analyze the resulting model; determine its properties; (5) decide on performance specification; (6) decide on the type of controller to be used; (7) design a controller to meet the specification, if possible; if not, modify the specification or generalize the type of controller sought; (8) simulate the resulting controlled system, either on a computer or in a pilot plant; (9) repeat from step 1 if necessary; (10) choose hardware and software and implement the controller; and (11) tune the controller on-line if necessary. From the foregoing steps, system modeling and sensor design are crucial for control system design

APPENDIX B

STATISTIC METHOD IN THE RESEARCH

Tissue engineering is multi-disciplinary subject that employs technology from engineering and mathematics to biological systems. This technology applies statistics especially in designing experiments. An experiment is a test or series of tests in which purposeful changes are made to the input variables of a process or system so that one may observe and identify the reasons for the changes in the output or response.

To use the statistical approach in designing and analyzing an experiment, it is necessary that everyone involved in the experiment have a clear idea in advance of exactly what is to be studied, how the data are to be collected, and at least a qualitative understanding of how these data are to be analyzed.

The factor investigation into a single-factor model analysis of variance can be either quantitative or qualitative. The experimenter is frequently interested in developing an interpolation equation from the data. The general approach to fitting equations to data is regression analysis. In general, suppose that there is a single dependent variable or response y that depends on k independent or regression variables. The relationship between these variables is characterized by a mathematical model called the regression equation. In some instances, the experimenter knows the exact form of the true functional relationship between y and x, say $y=f(x)$. However, in most cases, the

true functional relationship is unknown, and the experimenter chooses an appropriate function to approximate *f(x)*.

APPENDIX C

MONTE CARLO SAMPLING ALGORITHMS

"Monte Carlo" (MC) is a collection of computational methods that simulate complex statistical behaviors. In the current thesis, we use Monte Carlo sampling algorithms to simulate the degradation process. This appendix will introduce some basic concept and simulation process by the MC technique.

Monte Carlo algorithms are non-deterministic methods for simulating various phenomena and they are widely applied (Barry, 2007). Here, an example on using MC algorithms is introduced to calculate the value of π (Beckmann, 1970). Based on this so called "integration by darts" instance, reader will understand the concept of using probabilistic techniques to construct an estimated result which may not be able to obtain analytically.

Consider a unit circle with diameter 1 that is inscribed in a square. Perform "throw darts" in the square and count the number that falls within the unit circle. The "throw" action is a random process. In other words, n pairs of numbers were randomly generated, where each member of the pair is chosen randomly to fall between 0 and 1 (see Fig. C.1).

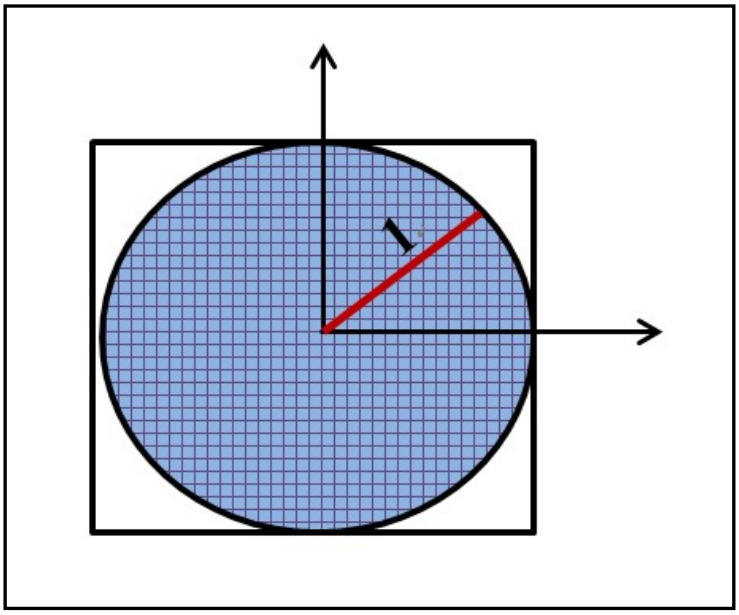

Figure C.1. Counting the number that "hit" within the first quadrant of the unit circle.

Count the number of n_{hit} that is less than a distance of one away from the origin. Clearly, if repeat this process long enough, there will be the following

$$\pi \approx 4\times\text{Area of circle in first quadrant} = \frac{4n_{hit}}{n} \qquad \text{(C-1)}$$

APPENDIX D

INTRODUCTION OF CARBON NANOTUBE (CNT)

CNTs can be viewed as a rolled-up grapheme strip. It is a closed cylinder as shown in Fig. D.1. The vectors $a_1$and a_2 generate the grapheme lattice (Fig. D.1) and they are found by Equation (D-1).

$$\begin{cases} a_1 = a(\sqrt{3}, 0) \\ a_2 = a(\sqrt{3}/2, 3/2) \end{cases} \quad \text{(D-1)}$$

where a=0.142nm is the carbon-carbon bond length. It can be observed from Fig. D.1 that $\mathrm{C} = \mathrm{n}a_1 + ma_2$. The radius of CNT is found by

$$\mathrm{R} = C/2\pi = \left(\sqrt{3}/2\pi\right)a\sqrt{n^2 + m^2 + nm} \quad \text{(D-2)}$$

There are two special cases shown in Fig. D.1. (A) “Zigzag” type: the circumferential vector lies along one of the two basis vectors; (B) “armchair” type: the circumferential vector is along the direction between the two basis vectors (n=m). Fig. D.1(c) shows a nanotube with arbitrary chirality (n,m), where the blue stripes generated by m≠n.

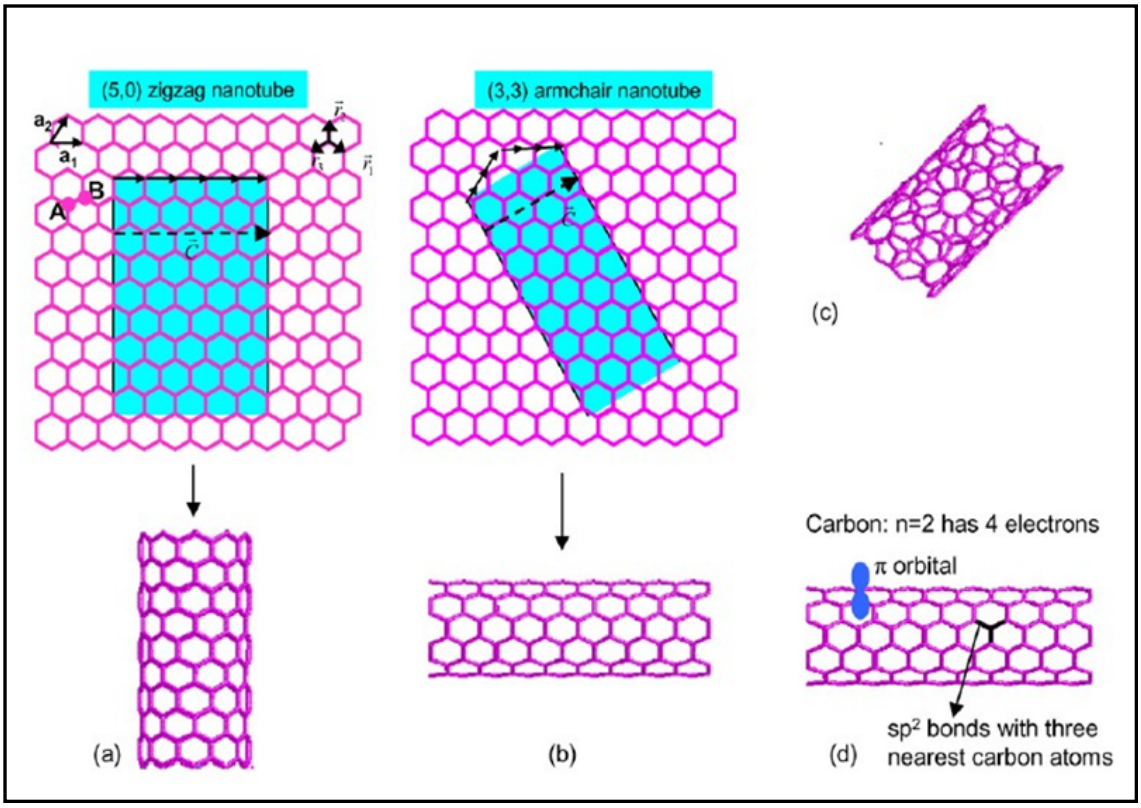

Figure D.1. CNTs structure: (a) a_1 and a_2 are the lattice vetros of grapheme; (b) creation of a (n,n) armchair nanotube; (c) a (n, m) chiral nanotube; (d) the bonding structure of a nanotube (Anantram & Leonard, 2005).

Electrically, CNTs can be either metallic or semi-conducting, depending upon the tube diameter and the chirality (the sheet direction in which the graphite sheet is rolled to form a nano-tube cylinder). The electrical properties of nanotubes are affected by distortions like bending and twisting. Pentagon-heptagon pair is introduced in CNTs by bending, which results in metal-metal and semiconductor-metal nano-scale junctions that can be used for nano-switches.

Mechanically, CNTs are currently the strongest known fibers because the carbon-carbon bond observed in graphite is one of the strongest in nature. Elastic properties of CNTs can be obtained from the experiment. The average value of Young's modulus is 1800 GPa. However, how to measure the tensile strength of CNTs is still a challenge.

There have been a plethora of applications of CNTs in the biomedical field alone. However, before such materials can be successfully incorporated into biomedical implants, drug/vaccine delivery vehicles or biosensors, there is a need to establish their biocompatibility. Other carbon-based biomaterials have demonstrated excellent long-term biocompatibility and biological performance in medical device applications. Clearly, these initial results urge caution when handling CNT.

APPENDIX E

THERMAL DEGRADATION

Table E.1(a) shows dry weight of chitosan film before and after the film was degraded subject to the thermal effect. Table E.1(b) shows the mass loss corresponding to degradation.

Talbe E.1. Degradation Data of Experiment-I

(a) Dry weight of chitosan film

Group A (37°C)		Group B (50°C)	
0 d (mg)	28 d (mg)	0 d (mg)	28 d (mg)
14.67	14.19	14.68	13.12
14.88	14.15	14.65	13.22
14.85	14.25	14.78	13.23
14.63	14.21	14.65	13.31
14.89	14.28	14.84	13.35

(b) Mass loss of chitosan film

Group A (37°C) (%)	Group B (50°C) (%)
3.27	10.62
4.91	9.76
4.041	10.48
2.871	9.15
4.09	9.37

Table E.2 shows the output of one-sample t-test by SPSS. (1) one-sample statistics;

(2) ANOVA table.

Talbe E.2. Output of One-Sample T-test SPSS

(a) One-Sample Statistics

	N	Mean	Std. Deviation	Std. Error Mean
A1	5	14.7840	.12402	.05546
A2	5	14.2160	.05079	.02272
B1	5	14.7200	.08573	.03834
B2	5	13.2660	.12300	.05501

(b) One-Sample Test

	Test Value = 0					
	t	df	Sig. (2-tailed)	Mean Difference	95% Confidence Interval of the Difference	
					Lower	Upper
A1	266.562	4	.000	14.78400	14.6300	14.9380
A2	625.825	4	.000	14.21600	14.1529	14.2791
B1	383.927	4	.000	14.72000	14.6135	14.8265
B2	241.160	4	.000	13.26600	13.1133	13.3187

Table E.3 shows the output of paired-sample t-test by SPSS

Talbe E.3. Output of Paired-Sample t-test

(a) Paired Samples Statistics

		Mean	N	Std. Deviation	Std. Error Mean
Pair 1	A	3.8372	5	.79122	.35385
	B	9.8777	5	.65981	.29508

(b) Paired Samples Correlations

	N	Correlation	Sig.
Pair 1 A & B	5	.072	.909

(c) Paired Samples Test

	Paired Differences					t	df	Sig. (2-tailed)
	Mean	Std. Deviation	Std. Error Mean	95% Confidence Interval of the Difference				
				Lower	Upper			
Pair 1 A – B	-6.04050	.99327	.44420	-7.27381	-4.80719	-13.598	4	.000

APPENDIX F

THERMAL-ENZYMATIC HYDROLYSIS

Table F.1(a) shows the dry weight of chitosan film before and after degradation experiment; table F.1(b) shows mass loss of chitosan films after degradation experiment.

Table F.1. Degradation Data of Experiment-II

(a) Dry weight of chitosan films.

37°C				50°C			
Geoup A (Control)		Gtoup B (Lysozyme)		Group C (Control)		Group D (Lysozyme)	
0 h (mg)	72 h (mg)	0 h (mg)	72 h (mg)	0 h (mg)	72 h (mg)	0 h (mg)	72 h (mg)
14.7	14.69	14.65	9.98	14.64	14.55	14.68	2.65
14.75	14.74	14.68	9.99	14.68	14.65	14.69	2.47
14.77	14.75	14.69	10.02	14.75	14.72	14.73	3.89
14.8	14.79	14.74	10.03	14.75	14.68	14.75	4.11
14.84	14.77	14.85	10.25	14.88	14.84	14.87	3.55

(b) Mass loss of chitosan films

37°C		50°C	
Group A (Control) (%)	Group B (Lysozyme) (%)	Group C (Control) (%)	Group D (Lysozyme) (%)
0.07	31.88	0.62	81.95
0.06	31.95	0.21	83.19
0.14	31.79	0.23	73.59
0.11	31.95	0.47	72.14
0.47	30.98	0.27	76.13

Table E.2 shows the output of one-sample T-test of chitosan films'dry weight after 72h degradation.

Table F. 2. Output of One-Sample T-test

(a) One-Sample Statistics

	N	Mean	Std. Deviation	Std. Error Mean
GroupA1	5	14.7720	.05263	.02354
GroupA2	5	14.7480	.03768	.01685
GroupB1	5	14.7220	.07855	.03513
GroupB2	5	10.0540	.11149	.04986
GroupC1	5	14.7400	.09138	.04087
GroupC2	5	14.6880	.10569	.04727
GroupD1	5	14.7440	.07603	.03400
GroupD2	5	3.3340	.73694	.32957

(b) One-Sample Test

	Test Value = 0					
	t	df	Sig. (2-tailed)	Mean Difference	95% Confidence Interval of the Difference	
					Lower	Upper
GroupA1	627.602	4	.000	14.77200	14.7067	14.8373
GroupA2	875.133	4	.000	14.74800	14.7012	14.7948
GroupB1	419.092	4	.000	14.72200	14.6245	14.8195
GroupB2	201.645	4	.000	10.05400	9.9156	10.1924
GroupC1	360.694	4	.000	14.74000	14.6265	14.8535
GroupC2	310.757	4	.000	14.68800	14.5568	14.8192
GroupD1	433.647	4	.000	14.74400	14.6496	14.8384
GroupD2	10.116	4	.001	3.33400	2.4190	4.2490

Table F.3 shows the output of paired-sample T-test of chitosan films' dry weight before and after 72h degradation.

Table F.3. Output of Paired-Sample T-test

(a) Paired Samples Statistics

		Mean	N	Std. Deviation	Std. Error Mean
Pair 1	GroupA1	14.7720	5	.05263	.02354
	GroupA2	14.7480	5	.03768	.01685
Pair 2	GroupB1	14.7220	5	.07855	.03513
	GroupB2	10.0540	5	.11149	.04986
Pair 3	GroupC1	14.7400	5	.09138	.04087
	GroupC2	14.6880	5	.10569	.04727
Pair 4	GroupD1	14.7440	5	.07603	.03400
	GroupD2	3.3340	5	.73694	.32957

(b) Paired Samples Correlations

			N	Correlation	Sig.
Pair 1	GroupA1	& GroupA2	5	.885	.046
Pair 2	GroupB1	& GroupB2	5	.964	.008
Pair 3	GroupC1	& GroupC2	5	.973	.005
Pair 4	GroupD1	& GroupD2	5	.511	.379

(c) Paired Samples Test

		Paired Differences					t	df	Sig. (2-tailed)
		Mean	Std. Deviation	Std. Error Mean	95% Confidence Interval of the Difference				
					Lower	Upper			
Pair 1	GroupA1 - GroupA2	.02400	.02608	.01166	-.00838	.05638	2.058	4	.109
Pair 2	GroupB1 - GroupB2	4.66800	.04147	.01855	4.61650	4.71950	251.682	4	.000
Pair 3	GroupC1 - GroupC2	.05200	.02683	.01200	.01868	.08532	4.333	4	.012
Pair 4	GroupD1 - GroupD2	11.41000	.70114	.31356	10.53942	12.28058	36.389	4	.000

Table F.4 shows main effect and interactions analysis in this factorial experiment.

Table F.4. Output of main effect and interaction analysis

(a) Temperature

Temperature	Mean	Std. Error	95% Confidence Interval	
			Lower Bound	Upper Bound
1	13.574	.029	13.393	13.655
2	11.877	.103	11.592	12.161

(b) Enzyme

Enzyme	Mean	Std. Error	95% Confidence Interval	
			Lower Bound	Upper Bound
1	14.737	.031	14.651	14.823
2	10.714	.099	10.439	10.988

(c) Time

Time	Mean	Std. Error	95% Confidence Interval	
			Lower Bound	Upper Bound
1	14.745	.033	14.653	14.836
2	10.706	.099	10.431	10.981

(d) Temperature×Time.

Temperature	Time	Mean	Std. Error	95% Confidence Interval	
				Lower Bound	Upper Bound
1	1	14.747	.029	14.667	14.827
	2	12.401	.030	12.318	12.484
2	1	14.742	.037	14.639	14.845
	2	9.011	.179	8.514	9.508

(e) Temperature×Enzyme

Temperature	Enzyme	Mean	Std. Error	95% Confidence Interval	
				Lower Bound	Upper Bound
1	1	14.760	.020	14.706	14.814
	2	12.388	.042	12.271	12.505
2	1	14.714	.044	14.592	14.836
	2	9.039	.174	8.556	9.522

(f) Time×Enzyme

Time	Enzyme	Mean	Std. Error	95% Confidence Interval	
				Lower Bound	Upper Bound
1	1	14.756	.032	14.668	14.844
	2	14.733	.034	14.637	14.829
2	1	14.718	.030	14.634	14.802
	2	6.694	.175	6.209	7.179

(g) Temperature×Time×Enzyme

Temperature	Time	Enzyme	Mean	Std. Error	95% Confidence Interval	
					Lower Bound	Upper Bound
1	1	1	14.772	.024	14.707	14.837
		2	14.722	.035	14.624	14.820
	2	1	14.748	.017	14.701	14.795
		2	10.054	.050	9.916	10.192
2	1	1	14.740	.041	14.627	14.853
		2	14.744	.034	14.650	14.838
	2	1	14.688	.047	14.557	14.819
		2	3.334	.330	2.419	4.249

APPENDIX G

LYSOZYME ACTIVITY EXPONENTIAL CURVE FITTING

Table G.1 shows model details of lysozyme activity exponential curve fitting.

Table G. 1. Model details

(a) Model Description

Model Name		MOD_1
Dependent Variable	1	Lysozyme
Equation	1	Exponential(a)
Independent Variable		Temperature
Constant		Included
Variable Whose Values Label Observations in Plots		Unspecified

a The model requires all non-missing values to be positive.

(b) Case Processing Summary

	N
Total Cases	7
Excluded Cases(a)	0
Forecasted Cases	0
Newly Created Cases	0

a Cases with a missing value in any variable are excluded from the analysis.

(c) Variable Processing Summary

		Variables	
		Dependent	Independent
		Lysozyme	Temperature
Number of Positive Values		7	7
Number of Zeros		0	0
Number of Negative Values		0	0
Number of Missing Values	User-Missing	0	0
	System-Missing	0	0

Table G.2 shows the Output of exponential curving fitting.

Table G. 2. Output of exponential curve fitting

(a) Model Summary

R	R Square	Adjusted R Square	Std. Error of the Estimate
.971	.942	.931	.271

The independent variable is Temperature.

(b) ANOVA

	Sum of Squares	df	Mean Square	F	Sig.
Regression	5.993	1	5.993	81.781	.000
Residual	.366	5	.073		
Total	6.360	6			

The independent variable is Temperature.

(c) Coefficients

	Unstandardized Coefficients		Standardized Coefficients	t	Sig.
	B	Std. Error	Beta		
Temperature	.110	.012	.971	9.043	.000
(Constant)	1.607	.761		2.111	.089

The dependent variable is ln(Lysozyme).

APPENDIX H

MATLAB COAD FOR MASS LOSS SIMULATION

```
%constants

T=37;
del_t=0;
t=0;
n=0;
ne=0;
DD=60;
N=10000;
L=20;
noPoints=1;
isPlotted=0;
for l=1:L
    %Generate 100 points randomly
    clear points;
    clear newOriginPoint;
    clear sortedPoints;
    clear sortedCol;
    clear sorter;
    for i=1:N
        %Get r and thetha
        r=rand;
        thetha=rand*2*pi;
        points(i,1)=r*cos(thetha);
        points(i,2)=r*sin(thetha);
        allPoints(noPoints,1)=points(i,1);
        allPoints(noPoints,2)=points(i,2);
        allPoints(noPoints,3)=l;
        noPoints=noPoints+1;
    end


    newOriginPoint(1,:)=points(1,:);
    for i=1:N
        points(i,3)=0;
        points(i,3)=points(i,3)+((points(i,1)-newOriginPoint(1,1))^2);
        points(i,3)=points(i,3)+((points(i,2)-newOriginPoint(1,2))^2);
        points(i,3)=points(i,3)^0.5;
```

```
        end
        [sortedCol, sorter] = sort(points(:,3),'ascend');
        sortedPoints=points(sorter,:);
        frac=0;
        del_t=0;
        n=0;
        ne=0;
        for i=1:N
            del_t=1.6065*exp(0.1105*T);
            t=t+del_t;
            ML=-160+10*DD-0.1*DD*DD;
            P=1-(ML/100);
            randNo=rand;
            if(randNo>P)
                ne=ne+1;
            end
            n=n+1;
        end
        frac=((n/N)*0.4)+((ne/n)*0.6);
        if(t>300000 && isPlotted==0)
            isPlotted=1;
            midPlotPoints=allPoints;
            figure(1);
            plot3(allPoints(:,1),allPoints(:,2),allPoints(:,3),'x');
            grid on;
        end
        if(frac<0.80)
            'Degradation did not happen'
        end
end

figure(2);
plot3(allPoints(:,1),allPoints(:,2),allPoints(:,3),'x');
grid on;
```